

# The Science Behind a Low-cost LED Sun Photometer

*Edoardo Milotti, Department of Physics, University of Trieste*



The Abdus Salam  
**International Centre  
for Theoretical Physics**



**UNIVERSITÀ**  
**DEGLI STUDI DI TRIESTE**

# The main themes:

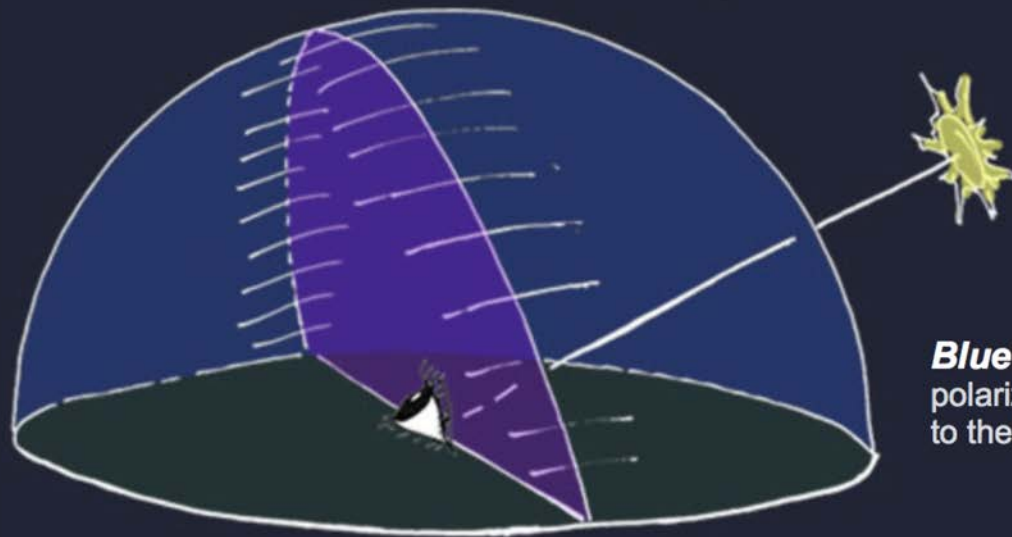
1. The physics of light scattering by small particles
2. Ray optics treatment of light scattering in large particles
3. The global patterns of dust transport



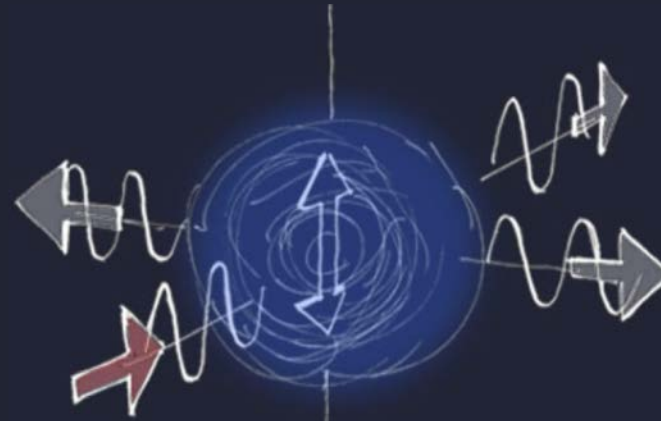
photo of the Golden Horn, Istanbul, by Rasid Tugral,  
from the Atmospheric Optics website,  
<https://www.atoptics.co.uk/fz1013.htm>

# Sky polarization

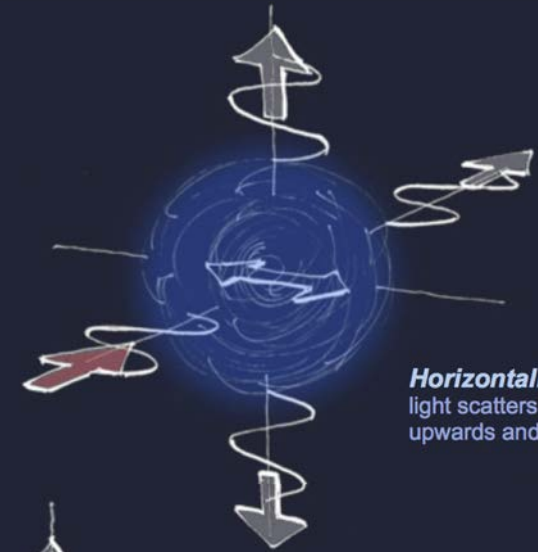
from <https://www.atoptics.co.uk/fz1013.htm>



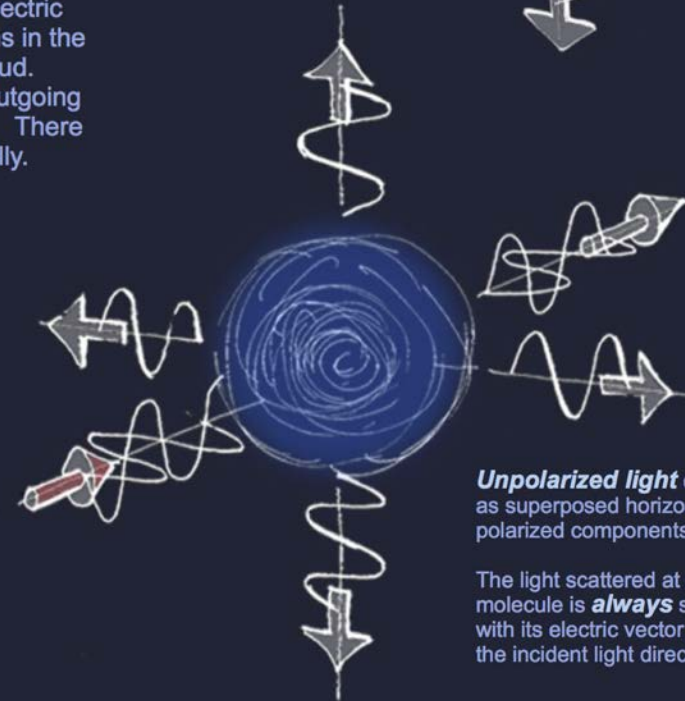
**Blue sky** is most strongly polarized in a plane at  $90^\circ$  to the sun.



**Vertically polarized light** interacting with an air molecule. Its varying electric field induces oscillations in the molecule's electron cloud. They in turn produce outgoing light equally polarized. There is little radiation vertically.



**Horizontally polarized** light scatters light mainly upwards and downwards.



**Unpolarized light** can be represented as superposed horizontal and vertical polarized components.

The light scattered at right angles by the molecule is **always** strongly polarized with its electric vector perpendicular to the incident light direction.



# Rayleigh scattering

Scattering of light by bound electrons (in contrast to Thomson/Compton scattering by free electrons)

Rayleigh developed the theory at the end of the 19th century, and he clarified many experimental facts, and several contrasting interpretations.

Lord Rayleigh (John William Strutt), 1842-1919, in a photograph he took himself around 1870.

from A. T. Young, "Rayleigh scattering", Phys. Today 35 (1), 42 (1982)




Irradiance

$$I = \frac{q^2 a^2 \sin^2 \theta}{16\pi^2 \epsilon_0 r^2 c^3}$$

Total irradiated  
power

$$W = \int_A I dA = \int_A \frac{q^2 a^2 \sin^2 \theta}{16\pi^2 \epsilon_0 r^2 c^3} 2\pi r^2 \sin \theta d\theta = \frac{q^2 a^2}{8\pi \epsilon_0 c^3} \int_0^\pi \sin^3 \theta d\theta$$

since  $\sin^3 \theta = \sin^2 \theta \times \sin \theta = (1 - \cos^2 \theta) \sin \theta$


$$\begin{aligned} \int_0^\pi \sin^3 \theta d\theta &= \int_0^\pi (1 - \cos^2 \theta) \sin \theta d\theta \\ &= \left( -\cos \theta + \frac{1}{3} \cos^3 \theta \right) \Big|_0^\pi = \frac{4}{3} \end{aligned}$$



$$P = \frac{q^2 a^2}{6\pi \epsilon_0 c^3}$$



## The case of the bound electron

Forcing electric field  $E_x(t) = E_0 \cos \omega t$

Elastically bound motion  $m\ddot{x} = -m\omega_0^2 x + qE_x$

Stationary solution  $-m\omega^2 x(t) = -m\omega_0^2 x(t) + qE_x(t)$

Explicit solution  $x(t) = \frac{qE_x(t)}{m(\omega_0^2 - \omega^2)}$


$$\ddot{x}(t) = -\frac{q\omega^2 E_x(t)}{m(\omega_0^2 - \omega^2)}$$

$$P = \frac{q^2}{6\pi\epsilon_0 c^3} a^2 = \frac{q^2}{6\pi\epsilon_0 c^3} \frac{q^2 \omega^4 E_x^2(t)}{m^2 (\omega_0^2 - \omega^2)^2}$$

# Rayleigh's "blue sky law"

$$\langle P \rangle = \frac{q^2}{6\pi\epsilon_0 c^3} \frac{q^2 \omega^4}{m^2 (\omega_0^2 - \omega^2)^2} \langle E_x^2 \rangle \propto \omega^4 \propto \frac{1}{\lambda^4}$$

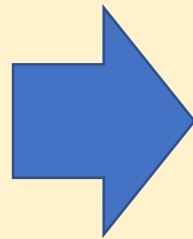
Average scattered power

$\omega_0 \gg \omega$

Frequency dependence

Wavelength dependence

Blue light:  $\lambda_1 \approx 450$  nm  
Red light:  $\lambda_2 \approx 650$  nm



$$\frac{1/\lambda_1^4}{1/\lambda_2^4} \approx 4.4$$

blue light is scattered about  
4 times more than red light



## Verification of the Rayleigh scattering cross section

Sayan Chakraborti<sup>a)</sup>

*Tata Institute of Fundamental Research, Mumbai, India*

(Received 12 February 2007; accepted 22 May 2007)

A simple experiment is described for the direct determination of the wavelength dependence of the Rayleigh scattering cross section using the classic example of the blue sky. Suggestions for inclusion into an undergraduate lab are discussed. © 2007 American Association of Physics Teachers.

[DOI: 10.1119/1.2752825]

Diagram illustrating the derivation of the Rayleigh scattering cross section from the lunar spectrum and the spectrum of the blue sky.

**Lunar spectrum equation:**

$$S_{\text{Moon}}(\lambda) = C_1 \alpha(\lambda) A_{\text{Moon}}(\lambda) S_{\text{Sun}}(\lambda)$$

Labels pointing to the equation:

- Lunar spectrum (points to  $S_{\text{Moon}}(\lambda)$ )
- Undetermined constant (points to  $C_1$ )
- Detector efficiency (points to  $\alpha(\lambda)$ )
- Lunar albedo (points to  $A_{\text{Moon}}(\lambda)$ )
- Solar spectrum (points to  $S_{\text{Sun}}(\lambda)$ )

**Spectrum of blue sky equation:**

$$S_{\text{Sky}}(\lambda) = C_2 \alpha(\lambda) \sigma_{\text{Rayleigh}}(\lambda) S_{\text{Sun}}(\lambda)$$

Labels pointing to the equation:

- Spectrum of blue sky (points to  $S_{\text{Sky}}(\lambda)$ )
- Undetermined constant (points to  $C_2$ )
- Rayleigh scattering cross section (points to  $\sigma_{\text{Rayleigh}}(\lambda)$ )

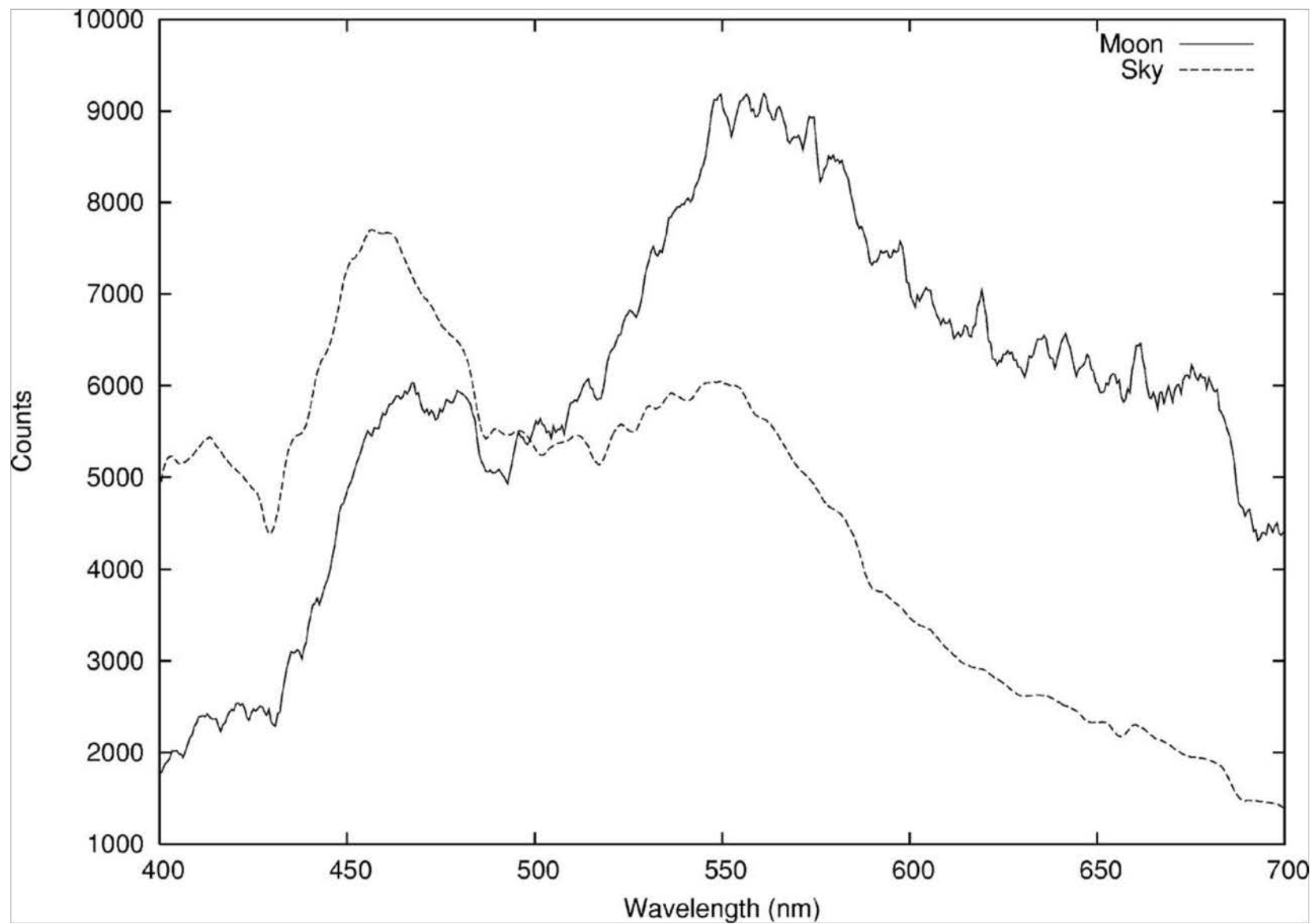


Fig. 1. Spectra of the moon and sky. Note that the peak is shifted toward shorter wavelengths in the sky spectra.

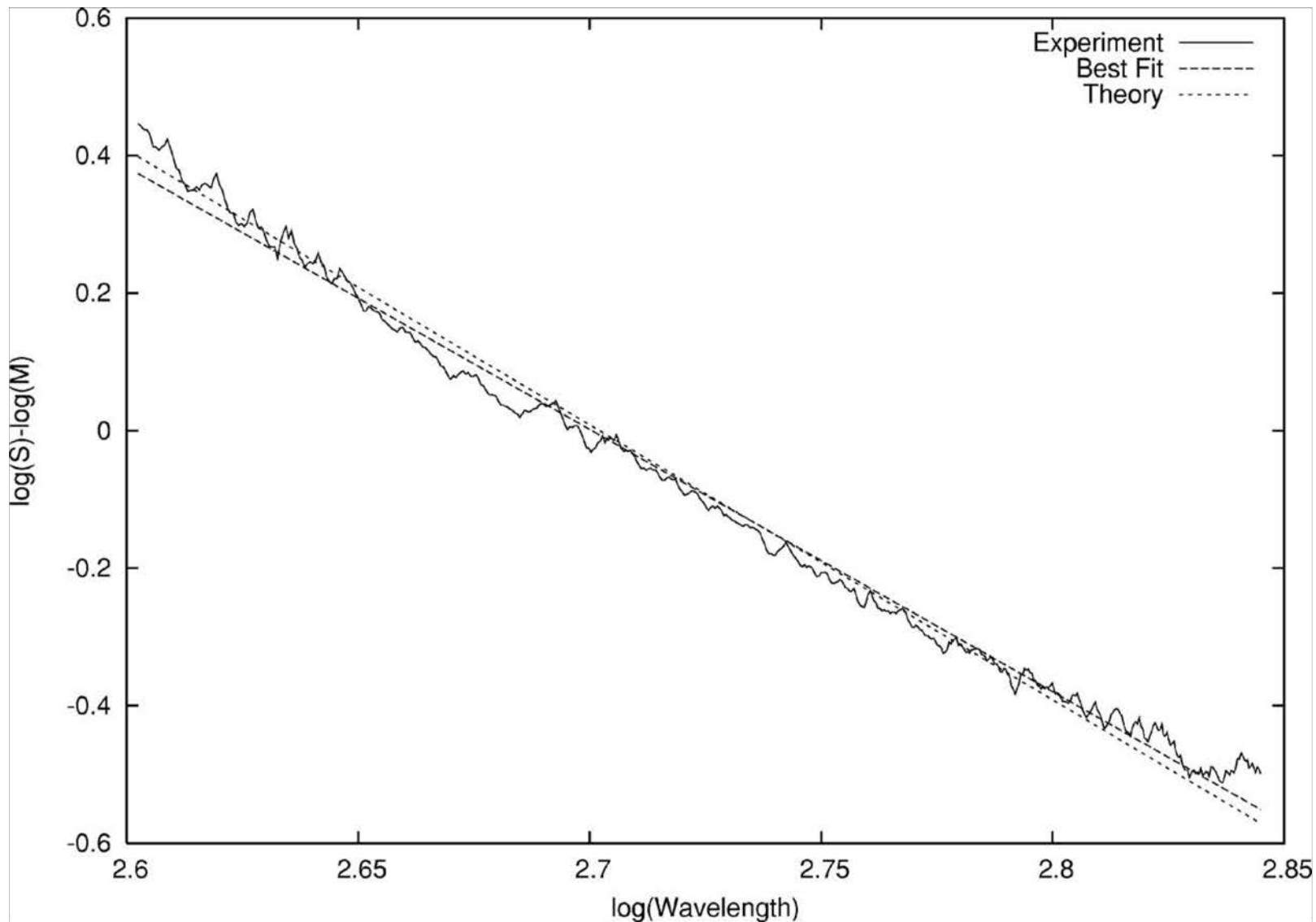
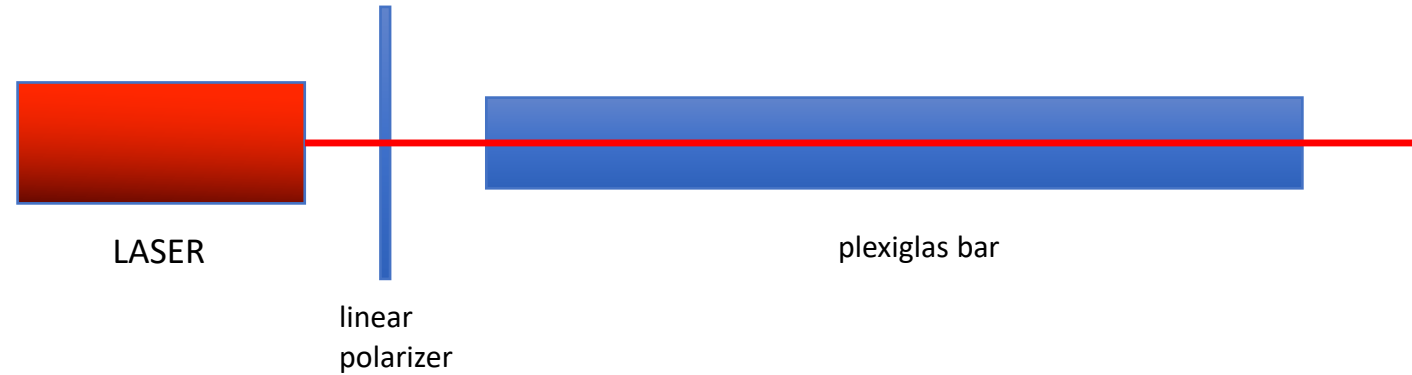
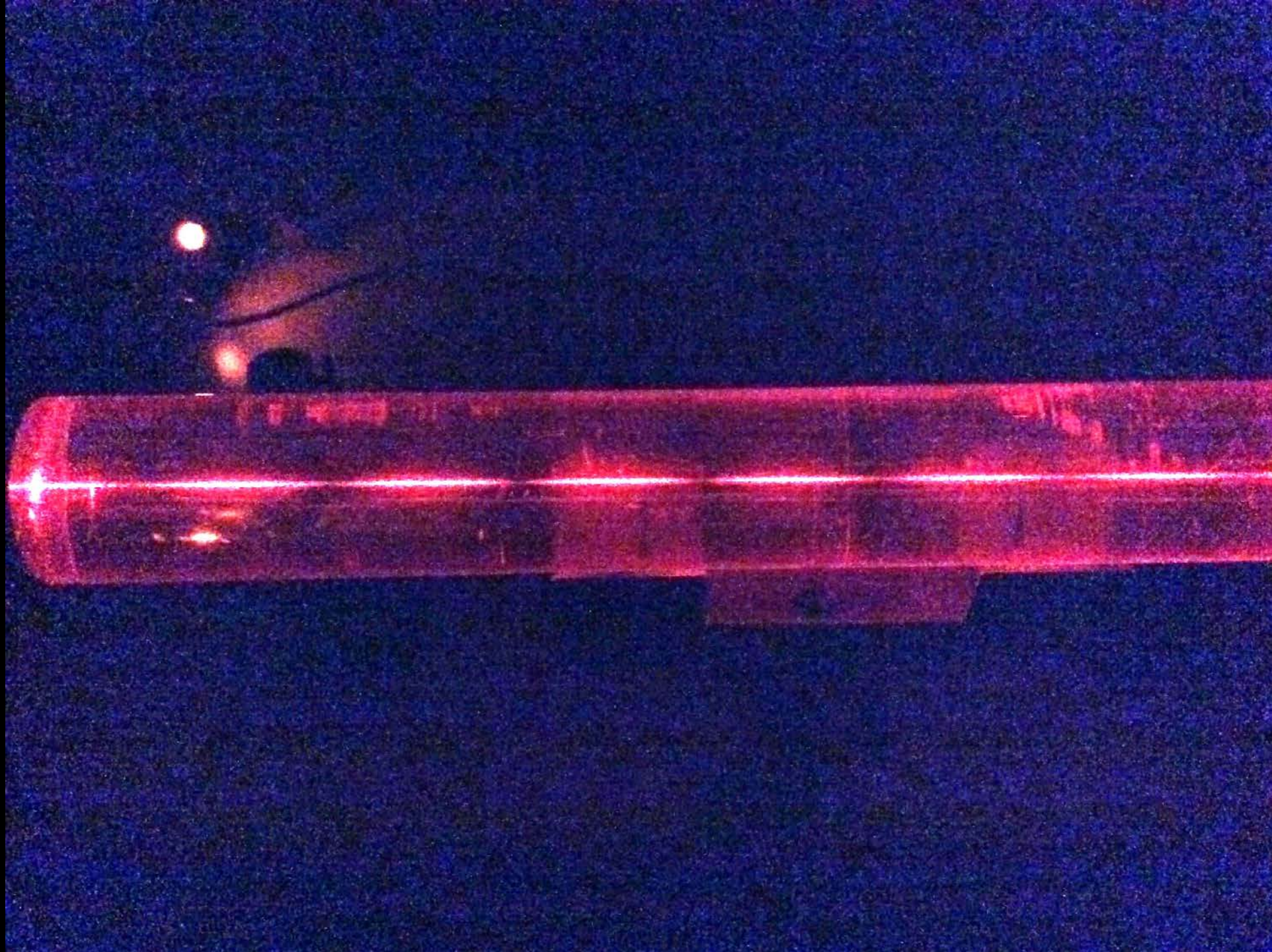


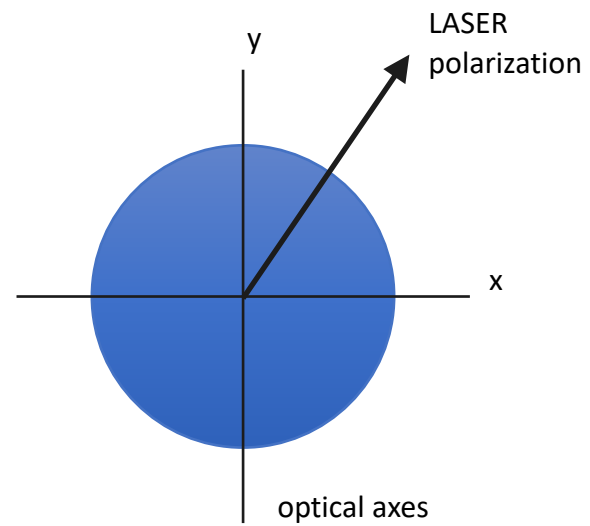
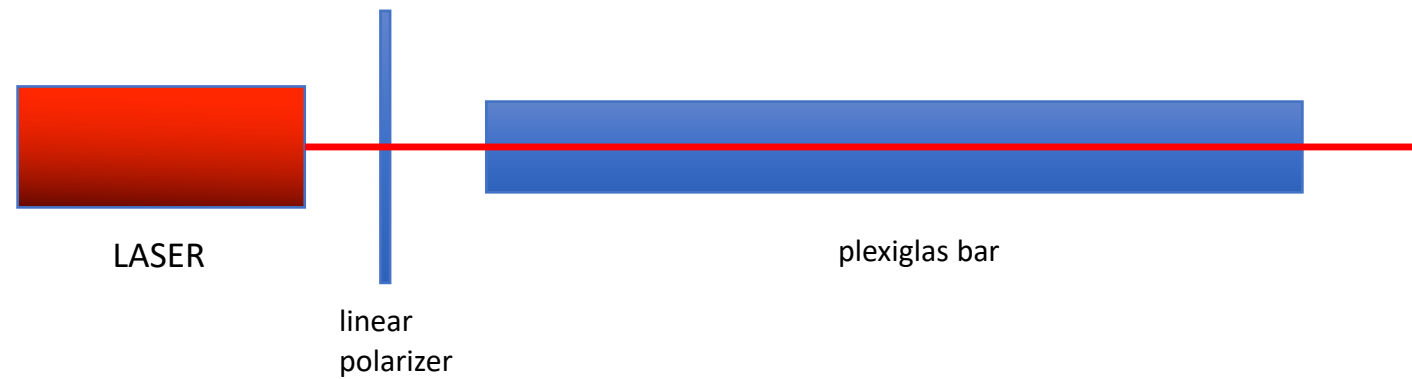
Fig. 2. Relative scattering cross section. Note the almost linear nature of the data points in a log-log plot, indicating a power law dependence.

# An interesting experiment with a plexiglas bar











# Ray optics treatment of light scattering in large particles

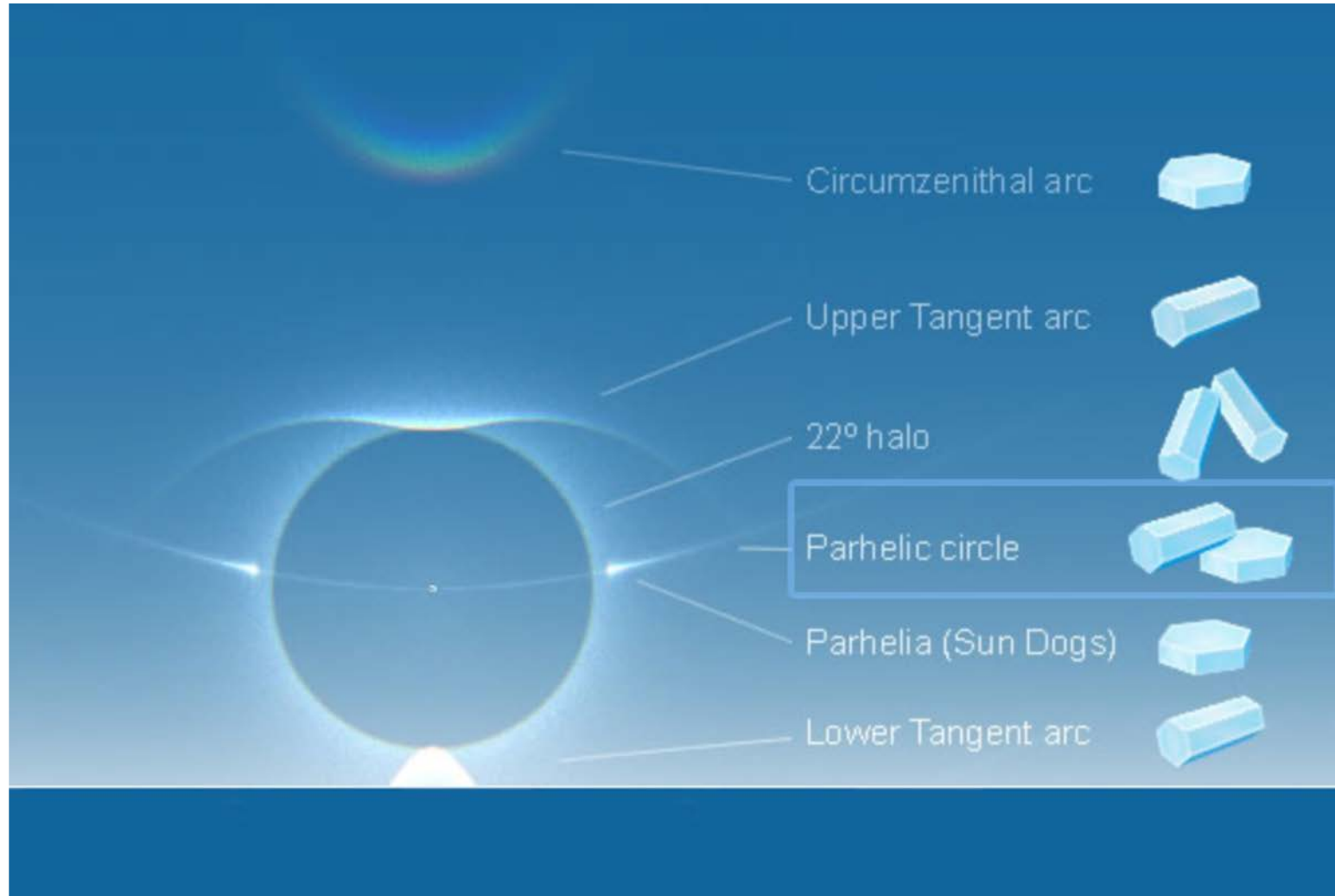




Image of ice halos in the morning of January 9 2015, in Red River, New Mexico, by Joshua Thomas (from <https://wordlesstech.com/magnificent-ice-halo-new-mexico/>)







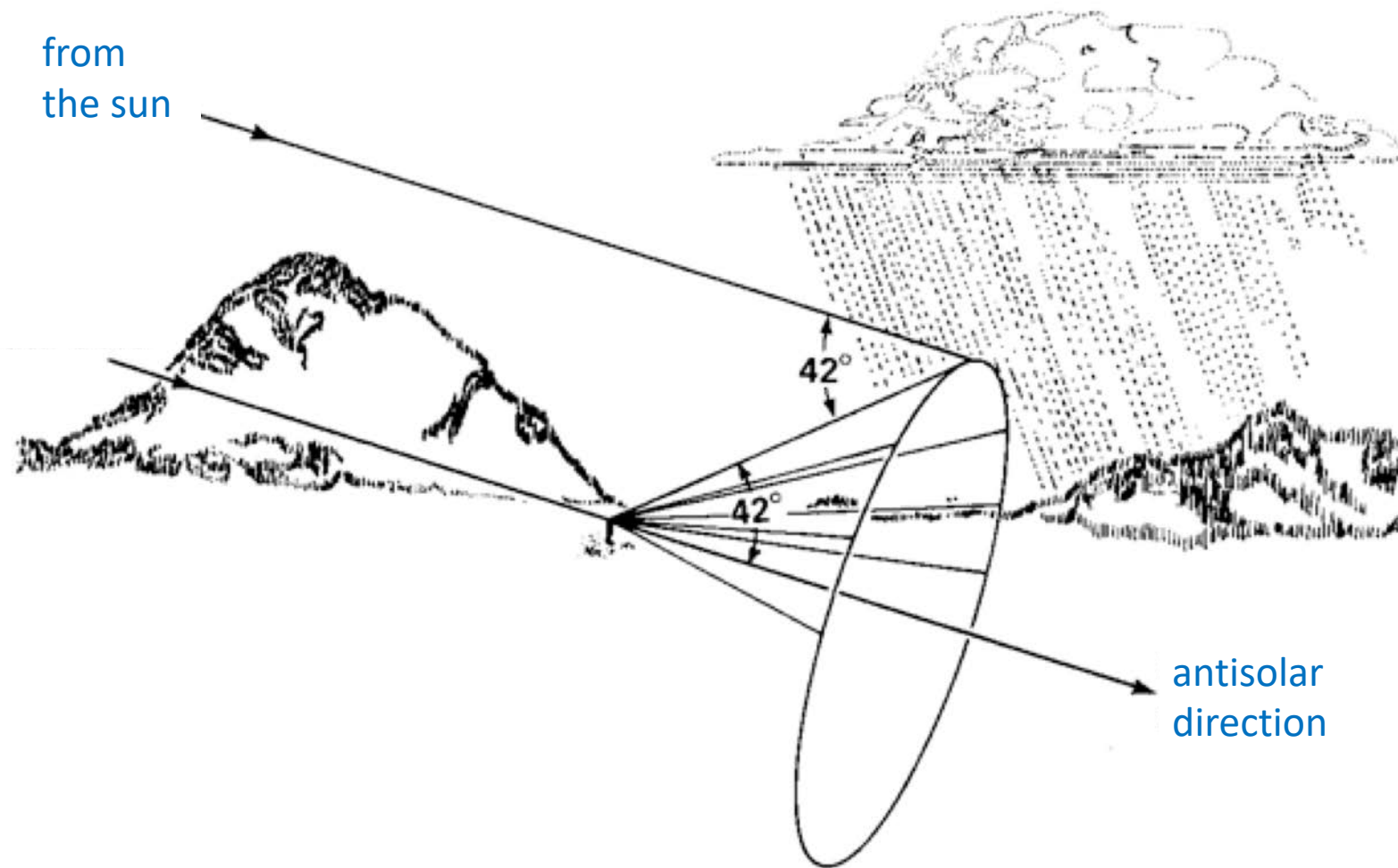




# Some observed features of natural rainbows

- Primary rainbow
  - blue-violet inside, red outside
  - opening angle about  $42^\circ$  with respect to the antisolar direction
- Secondary rainbow
  - red inside, blue outside
  - opening angle about  $51^\circ$ , less bright
- No tertiary rainbow
- Supernumerary arcs
- Sky is divided in regions with different brightness
  - Alexander's dark band
- Strong polarization effects
- Variable color
  - white bows





da R. Greenler: *Rainbows, Halos and Glories*, Cambridge Univ. Press (1980)

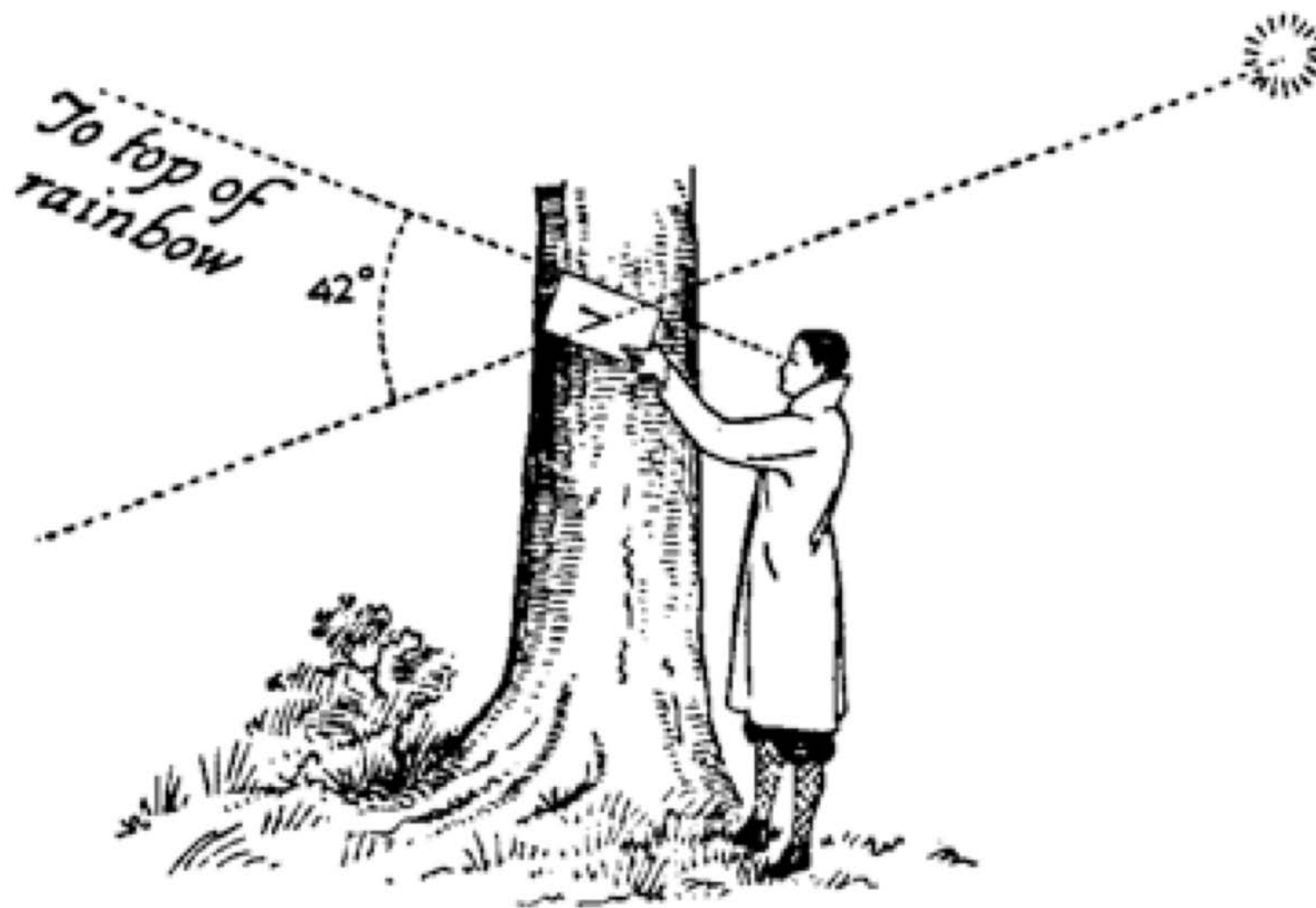
---

Diameter: 1–2 mm (0.04–0.08 in)	Very bright violet and vivid green; the bow contains pure red, but scarcely any blue. Spurious bows are numerous (five, for example), violet-pink alternating with green merging without interruption into the primary bow.
0.5 mm (0.02 in)	The red is considerably weaker. Fewer supernumerary bows, violet-pink and green again alternating.
0.2–0.3 mm (0.008–0.012 in)	No more red; for the rest, the bow is broad and well developed. The supernumerary bows become more and more yellow. If a gap occurs between the supernumerary bows, the diameter of the drops is 0.2 mm (0.008 in). If there is a gap formed between the primary bow and the first supernumerary bow, the diameter of the drop is less than 0.2 mm (0.008 in).
0.08–0.1 mm (0.003–0.004 in)	The bow is broader and paler, and only the violet is vivid. The first supernumerary bow is well separated from the primary bow and clearly shows white tints.
0.06 mm (0.0024 in)	The primary rainbow contains a distinct white stripe.
<0.05 mm (<0.002 in)	Mistbow (cf. § 150)

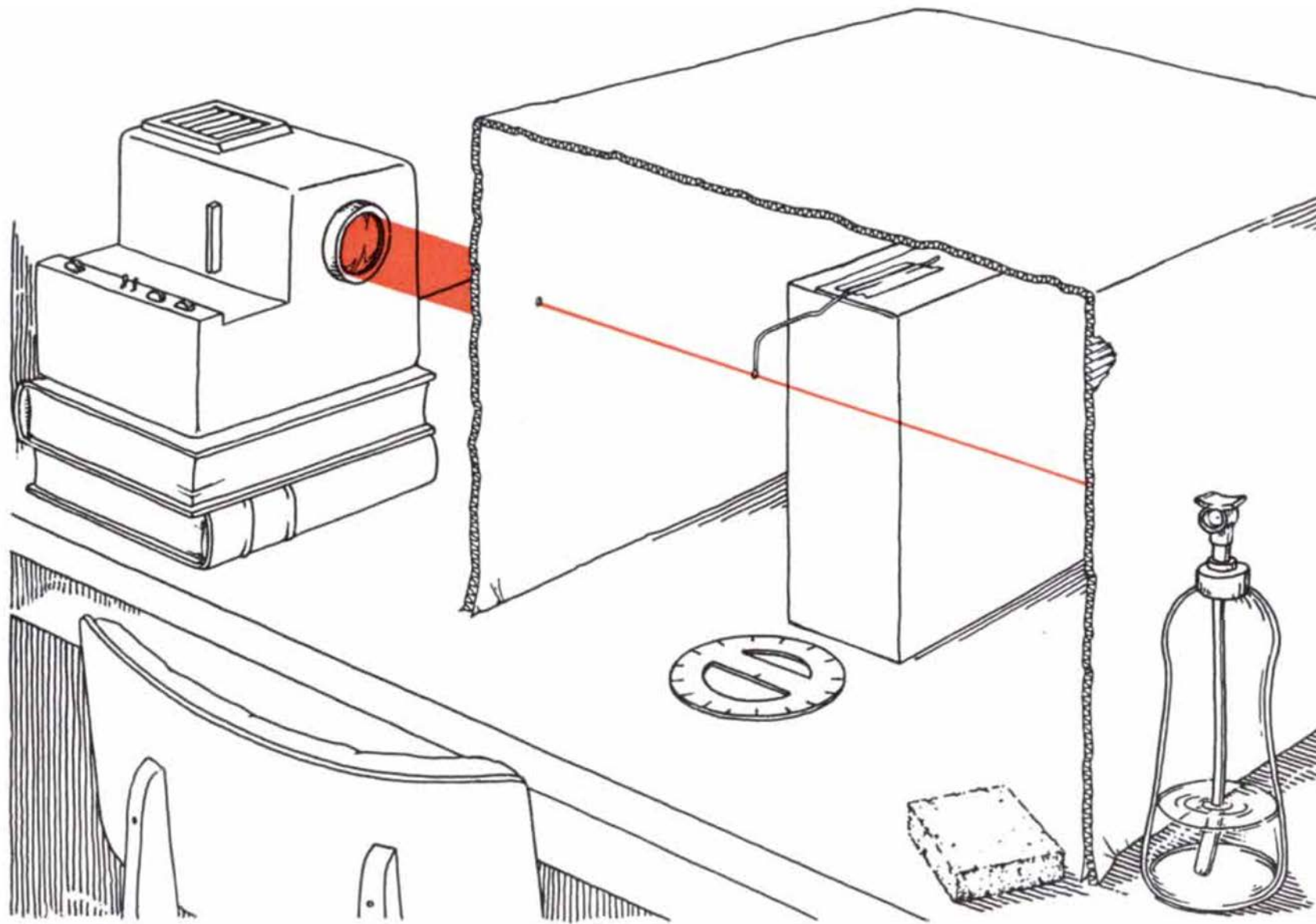
---



Rene Winter

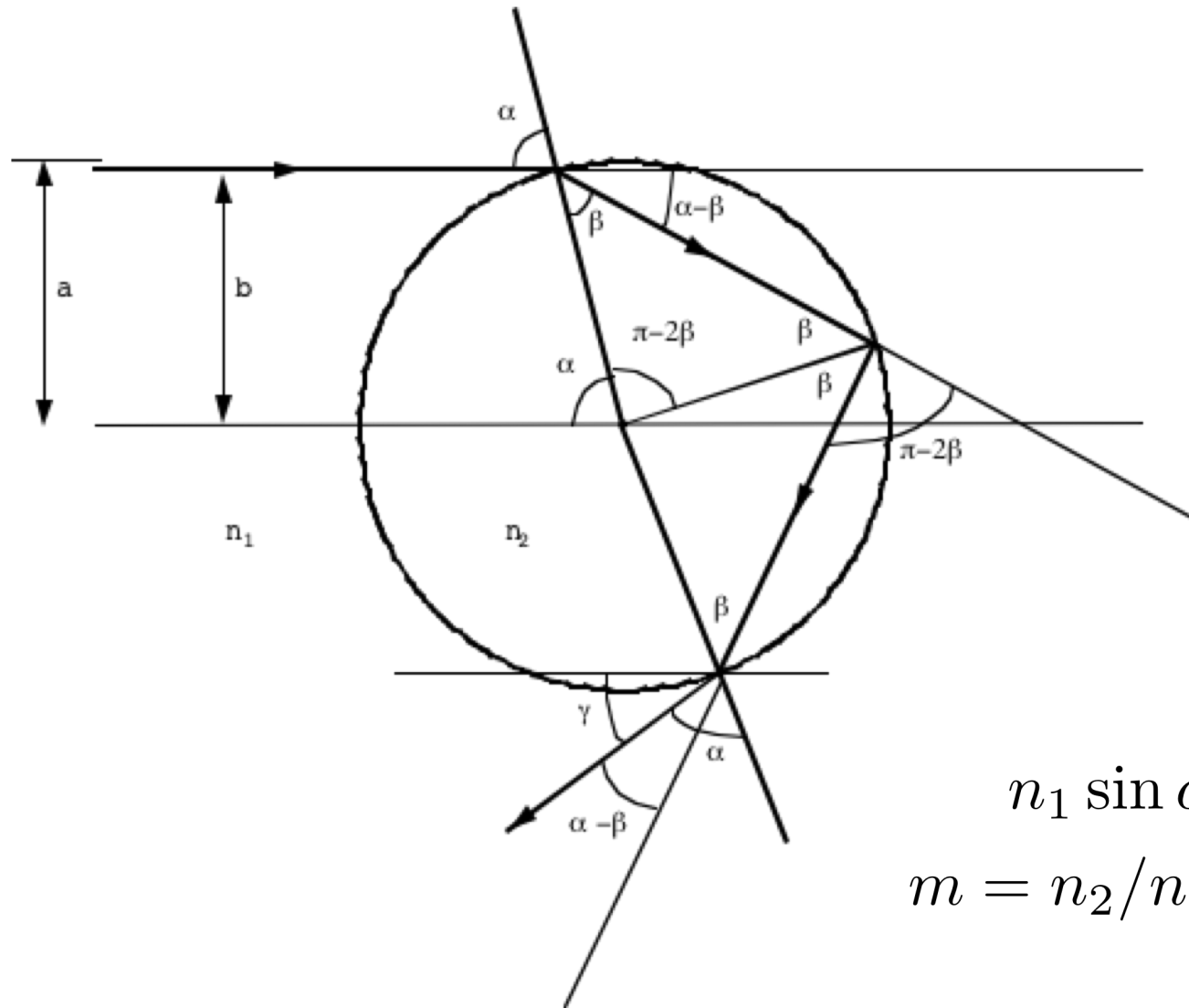


from M. Minnaert, *Light and Color in the Open Air*, Dover (1954)



*Apparatus for observing rainbows in a drop of water*

# Geometry of refractions and reflections inside a water droplet



$a$  = droplet radius  
 $b$  = impact parameter

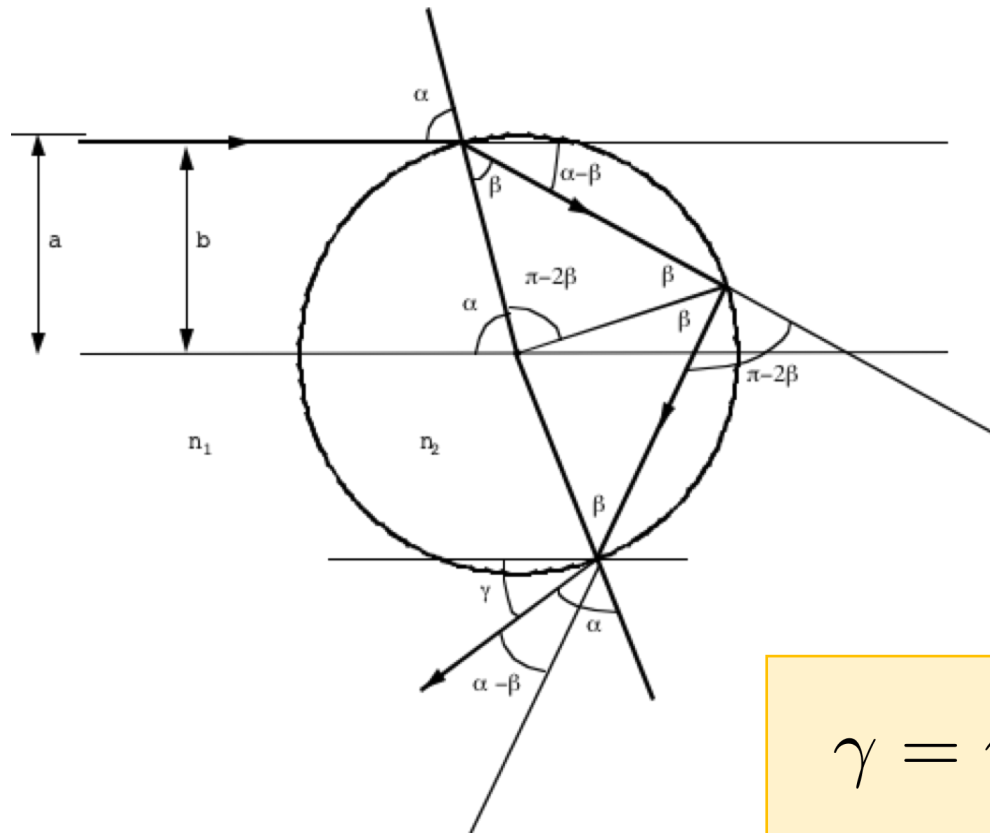
$$b = a \sin \alpha$$

$$n_1 \sin \alpha = n_2 \sin \beta$$

$$m = n_2/n_1 \Rightarrow \sin \alpha = m \sin \beta$$

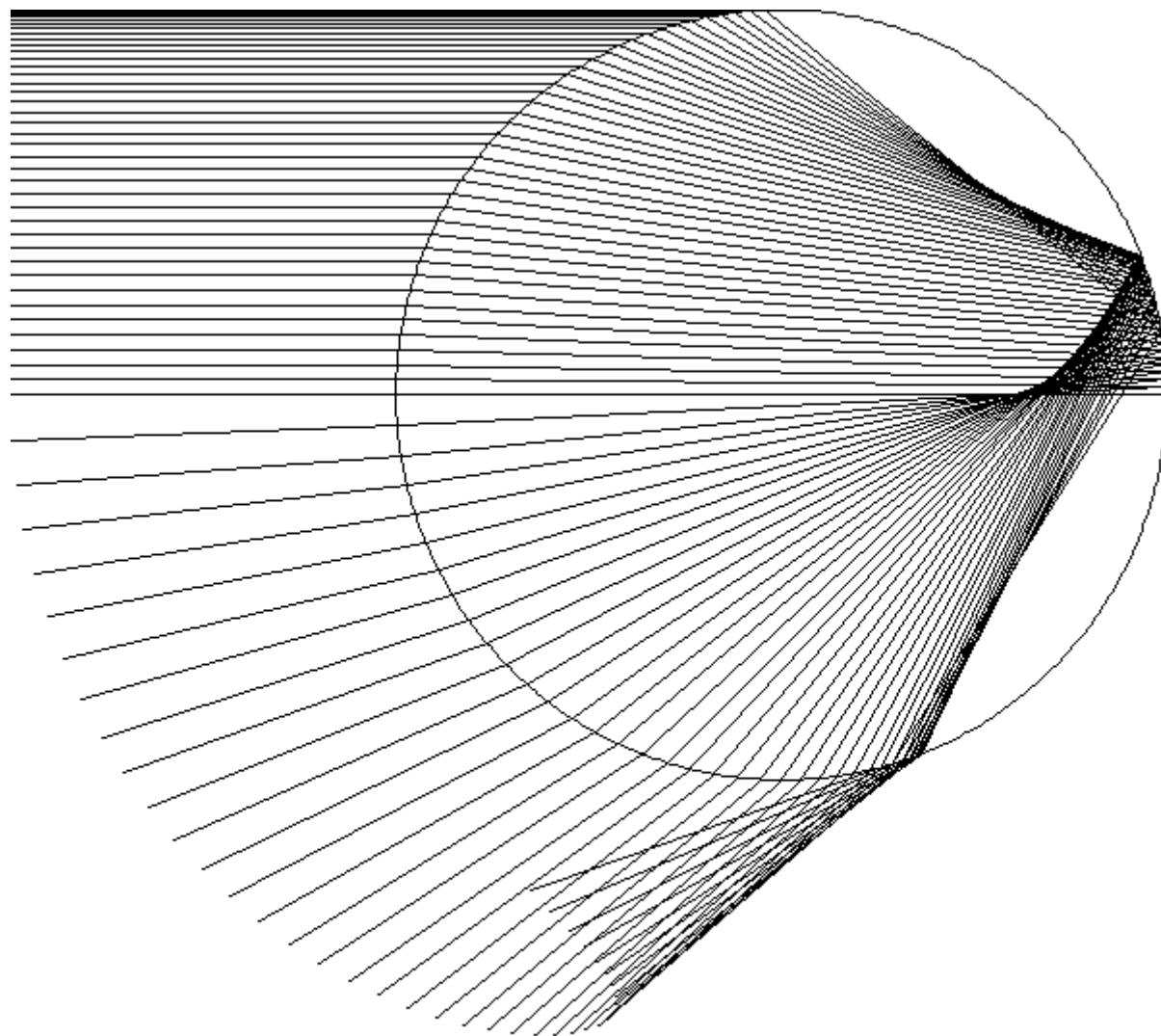
$$\beta = \arcsin \left( \frac{1}{m} \sin \alpha \right) = \arcsin \left( \frac{b}{ma} \right)$$

$$\begin{aligned}
 \left( \begin{array}{c} \text{total} \\ \text{rotation angle} \end{array} \right) &= \left( \begin{array}{c} \text{rotation due to} \\ \text{first refraction} \end{array} \right) + \left( \begin{array}{c} \text{rotation due} \\ \text{to reflection} \end{array} \right) + \left( \begin{array}{c} \text{rotation due to} \\ \text{second refraction} \end{array} \right) \\
 &= (\alpha - \beta) + (\pi - 2\beta) + (\alpha - \beta) \\
 &= \pi + 2\alpha - 4\beta
 \end{aligned}$$

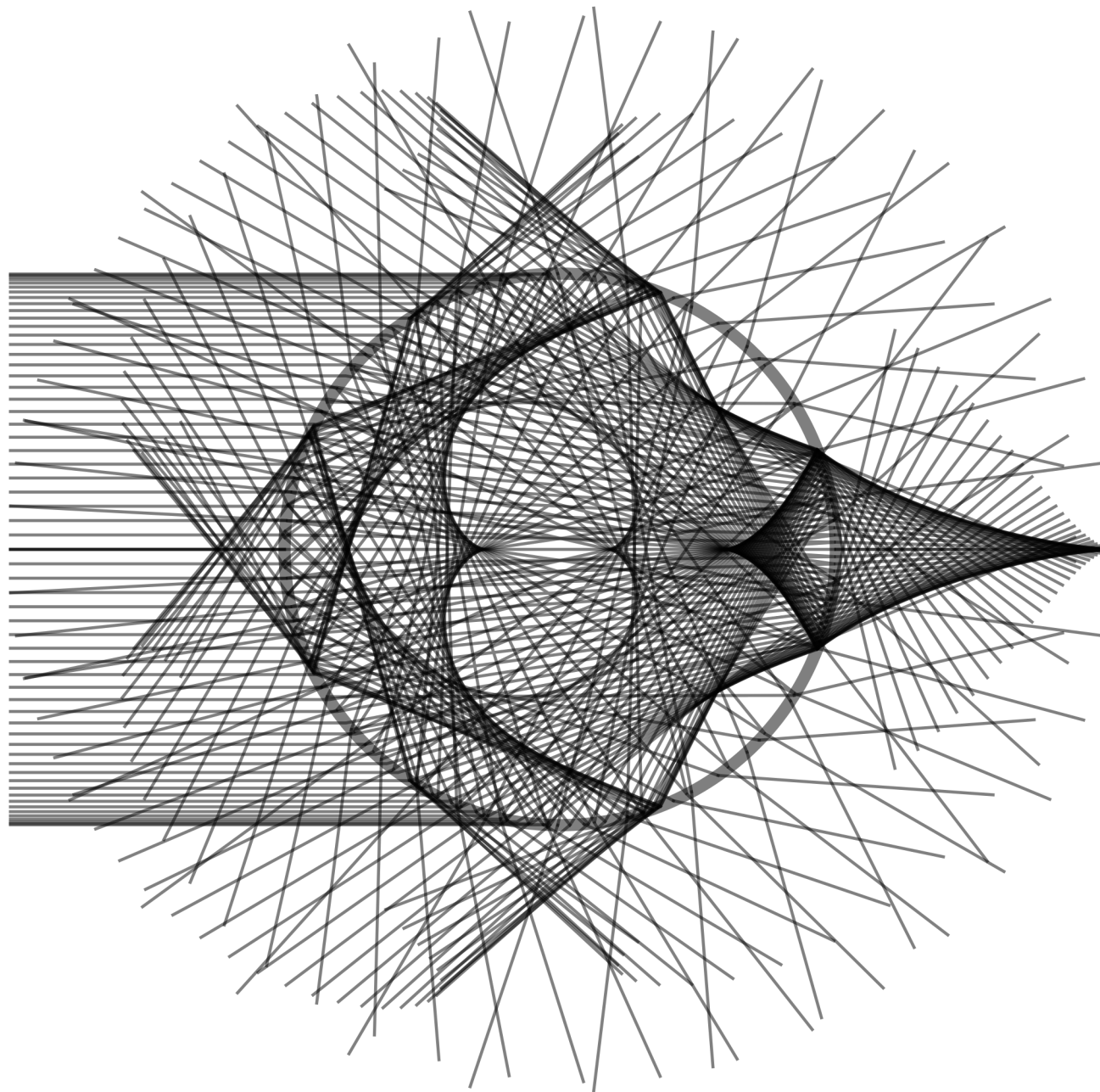


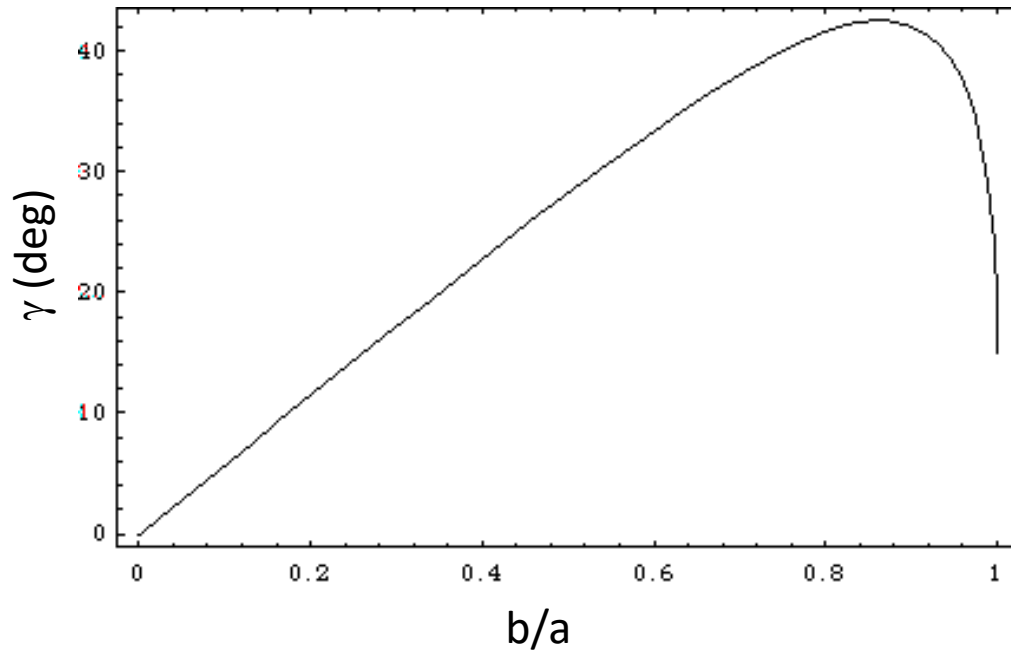
Rainbow angle

$$\gamma = \pi - (\text{total rotation angle}) = 4\beta - 2\alpha$$









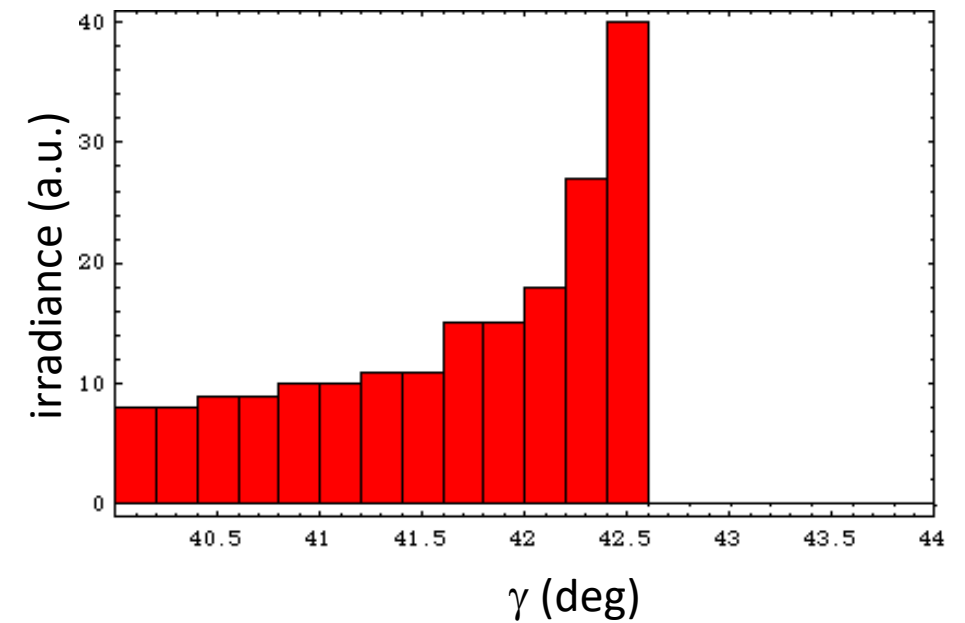
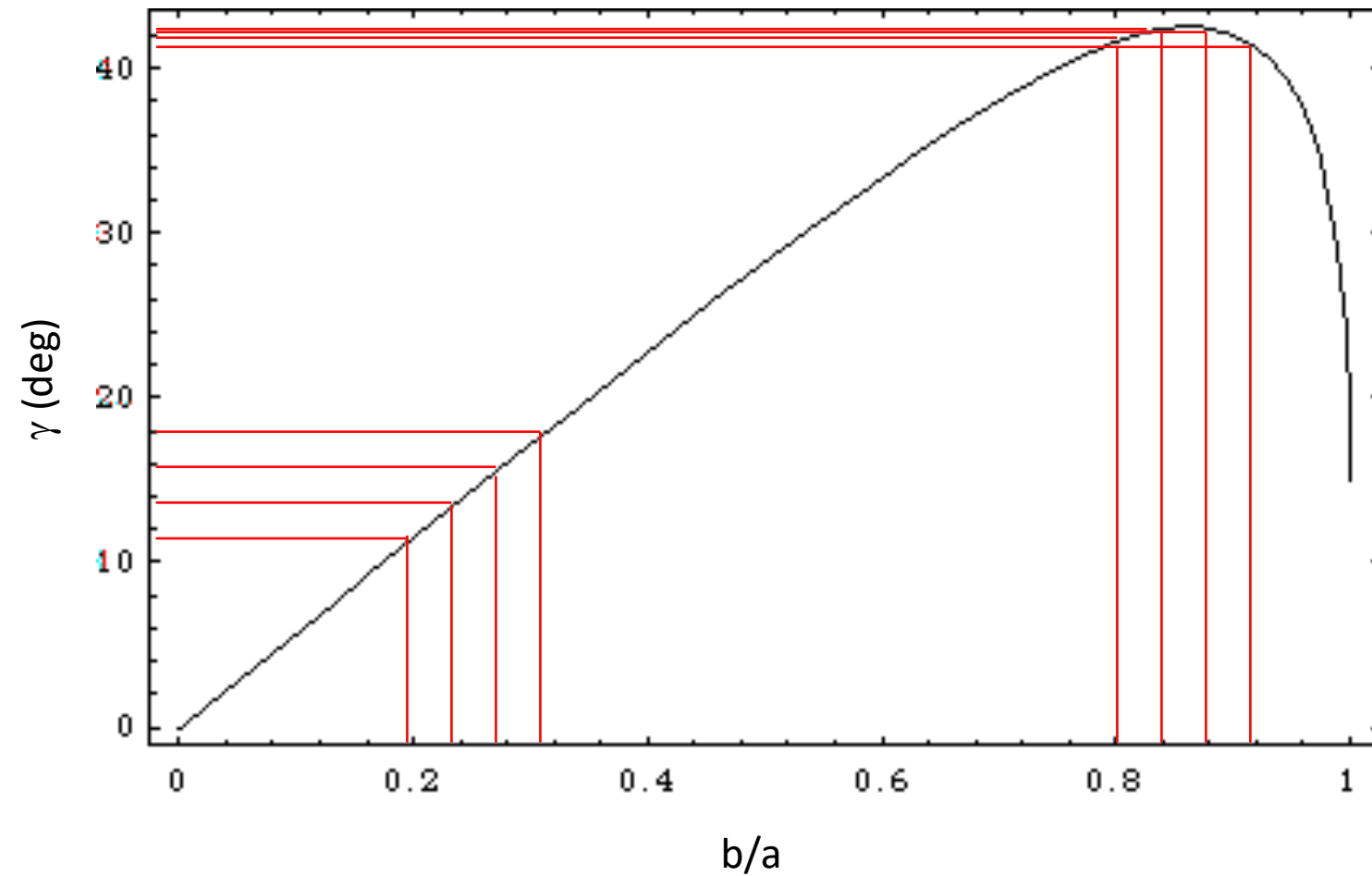
## Peak irradiance

$$\gamma = 4\beta - 2\alpha = 4 \arcsin\left(\frac{b}{ma}\right) - 2 \arcsin\left(\frac{b}{a}\right)$$

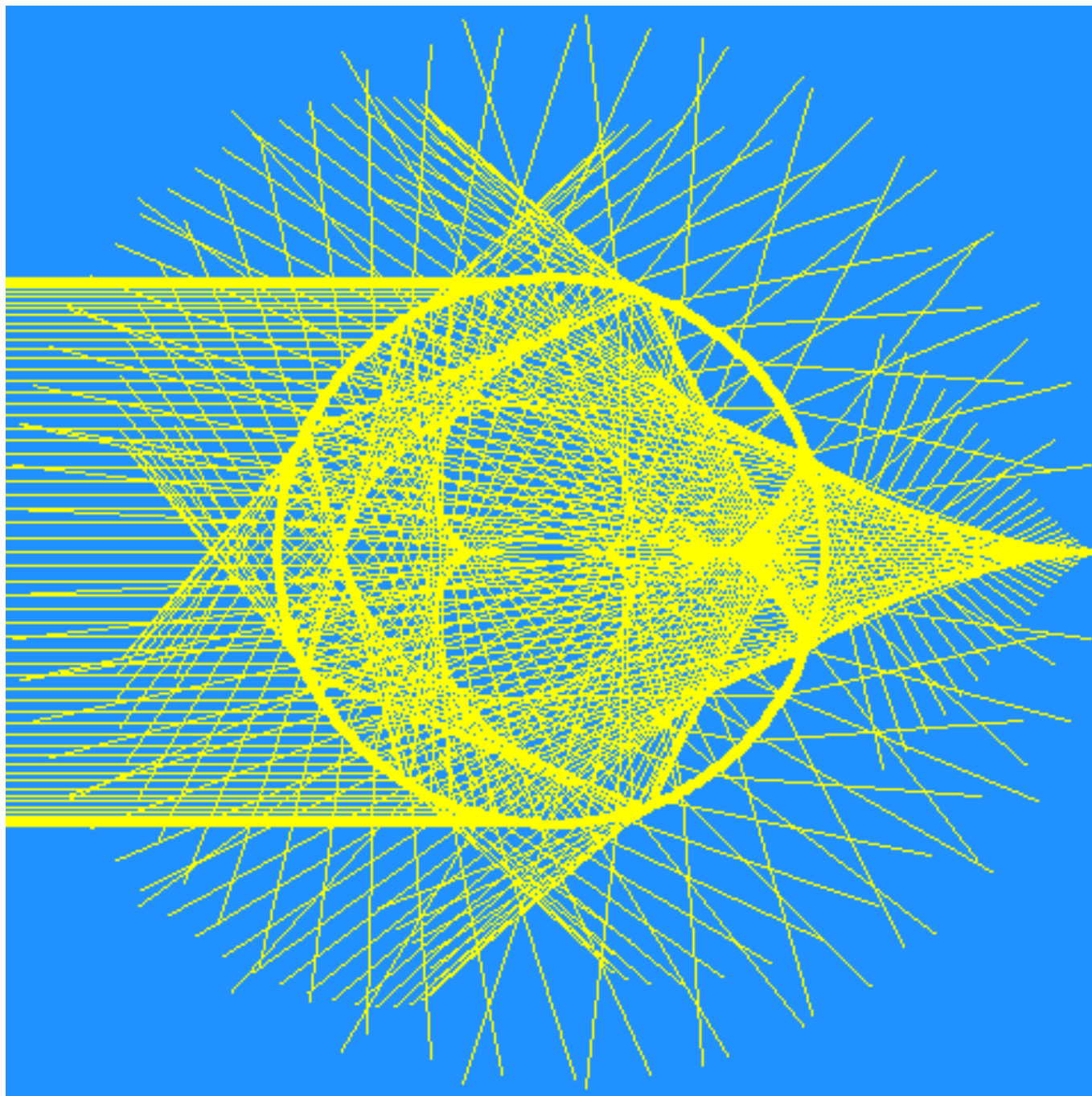
$$\frac{d\gamma}{db} = \frac{4}{ma} \times \left(1 - \frac{b^2}{m^2 a^2}\right)^{-1/2} - \frac{2}{a} \times \left(1 - \frac{b^2}{a^2}\right)^{-1/2}$$

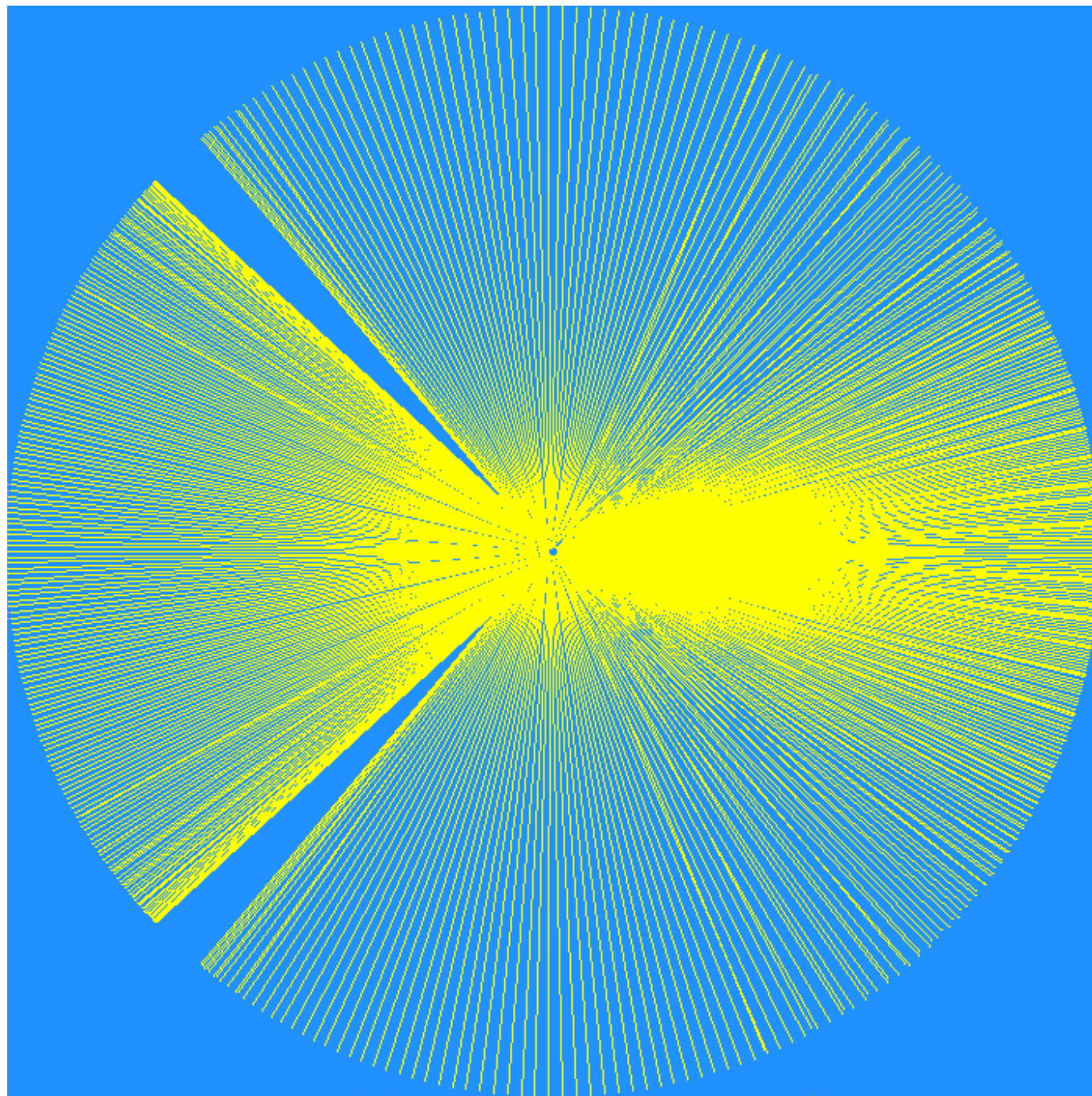
$$\frac{d\gamma}{db} = 0 \Rightarrow \frac{4}{m^2 a^2 - b^2} = \frac{1}{a^2 - b^2} \Rightarrow \frac{b}{a} = \sqrt{\frac{4 - m^2}{3}}$$

$$m \approx 1.33 \Rightarrow \begin{cases} b/a \approx 0.86 \\ \gamma \approx 42^\circ.5 \end{cases}$$



Irradiance proportional to density of light rays







## A homemade rainbow

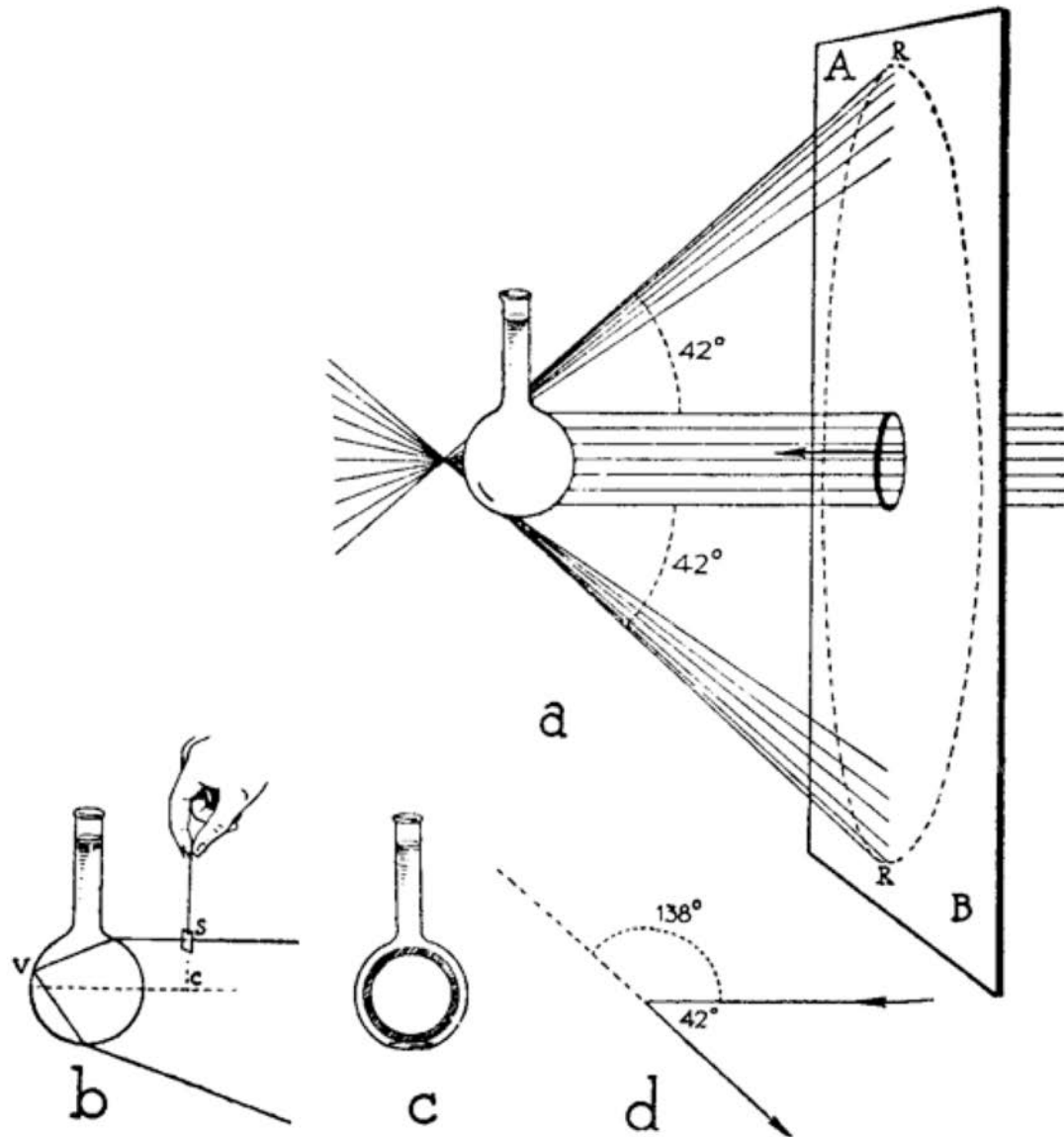
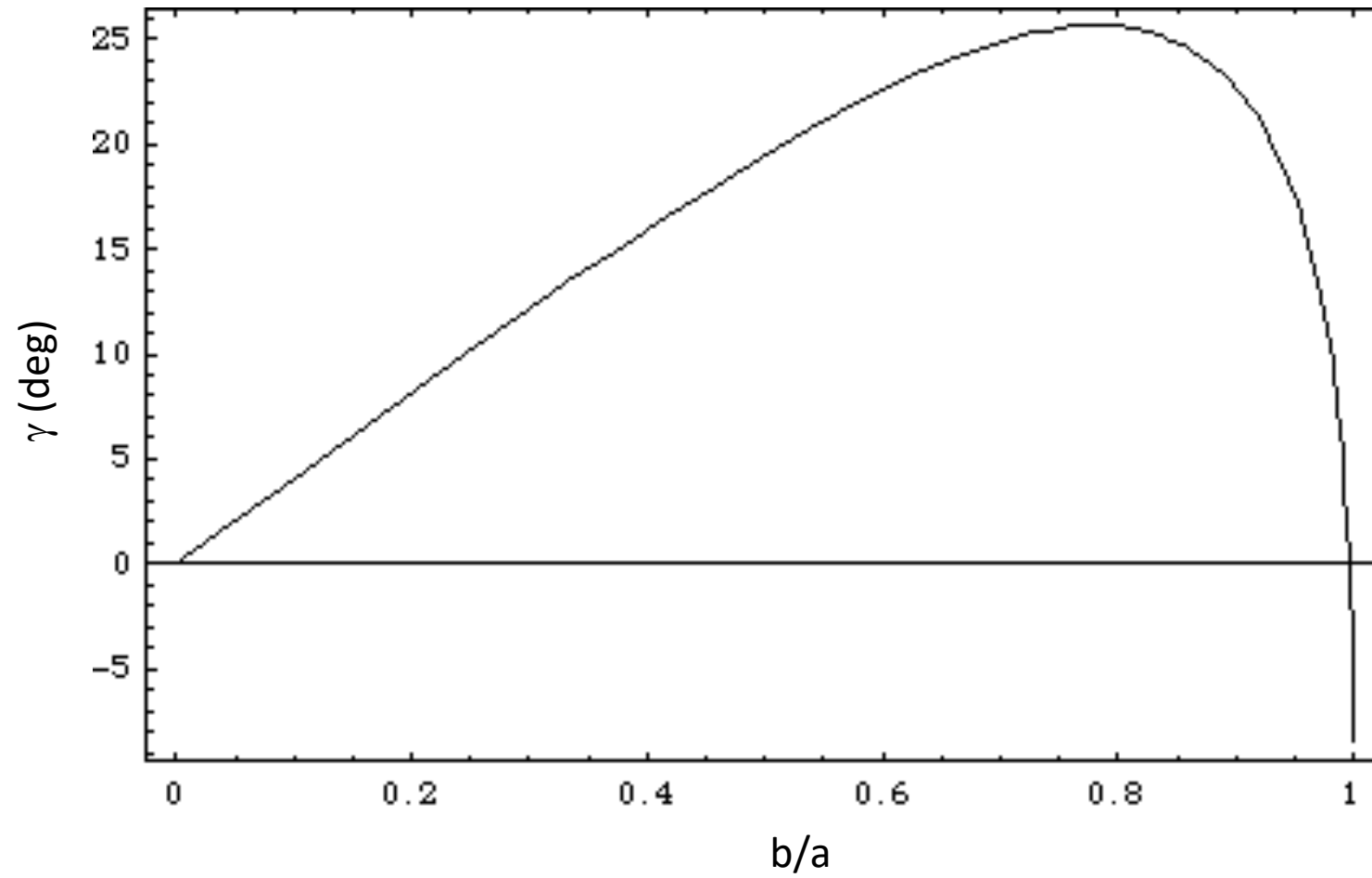


FIG. 109. Reproduction of a rainbow by means of a flask filled with water.

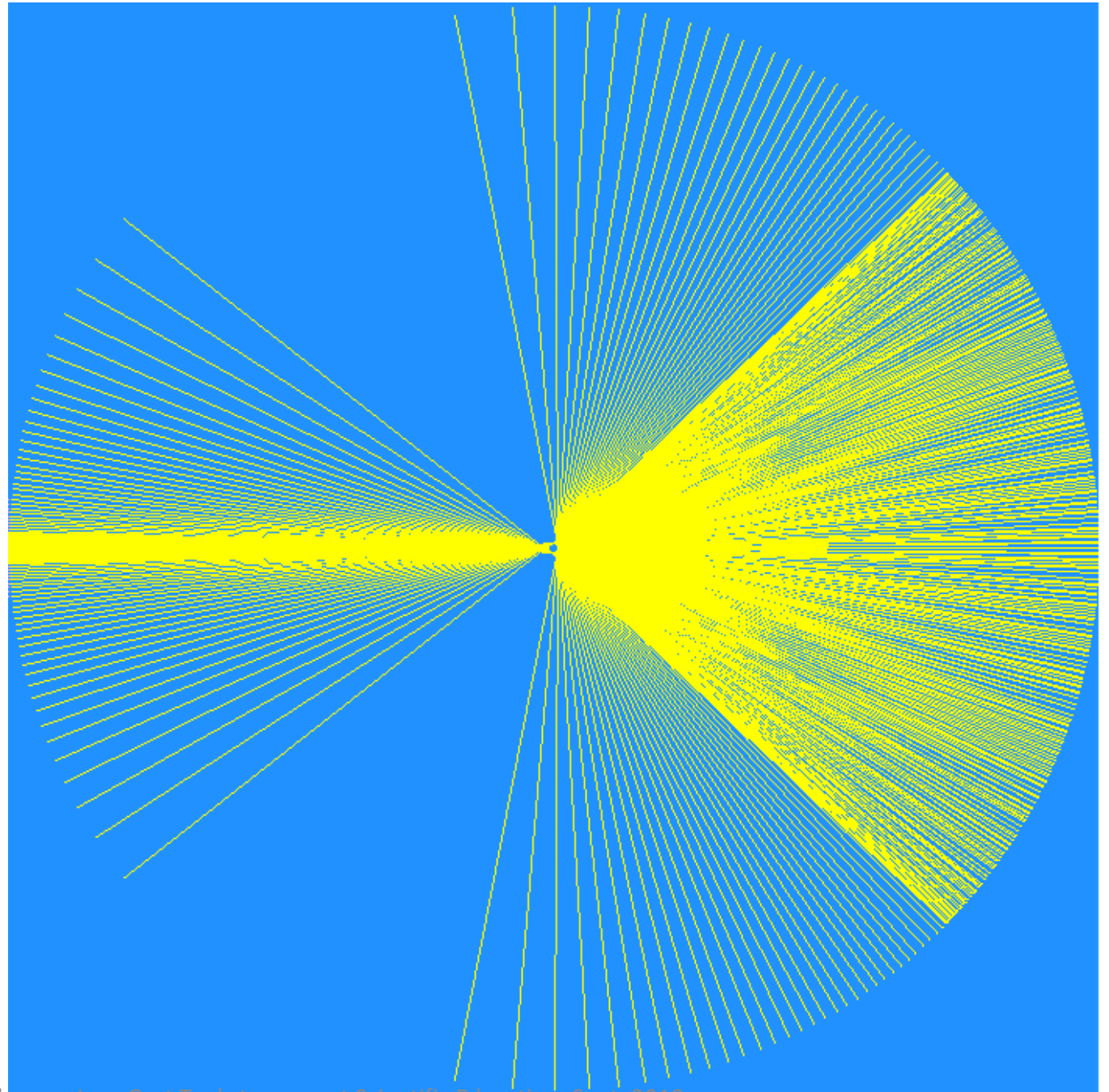
from M. Minnaert, *Light and Color in the Open Air*, Dover (1954)

## A glycerol rainbow ( $n \approx 1.47$ )



$\gamma$  peaks at  $\frac{b}{a} = \sqrt{\frac{4 - m^2}{3}}$

so that when  $m=2$ , all the reflected light bounces back at the source.

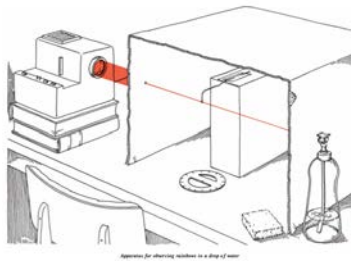




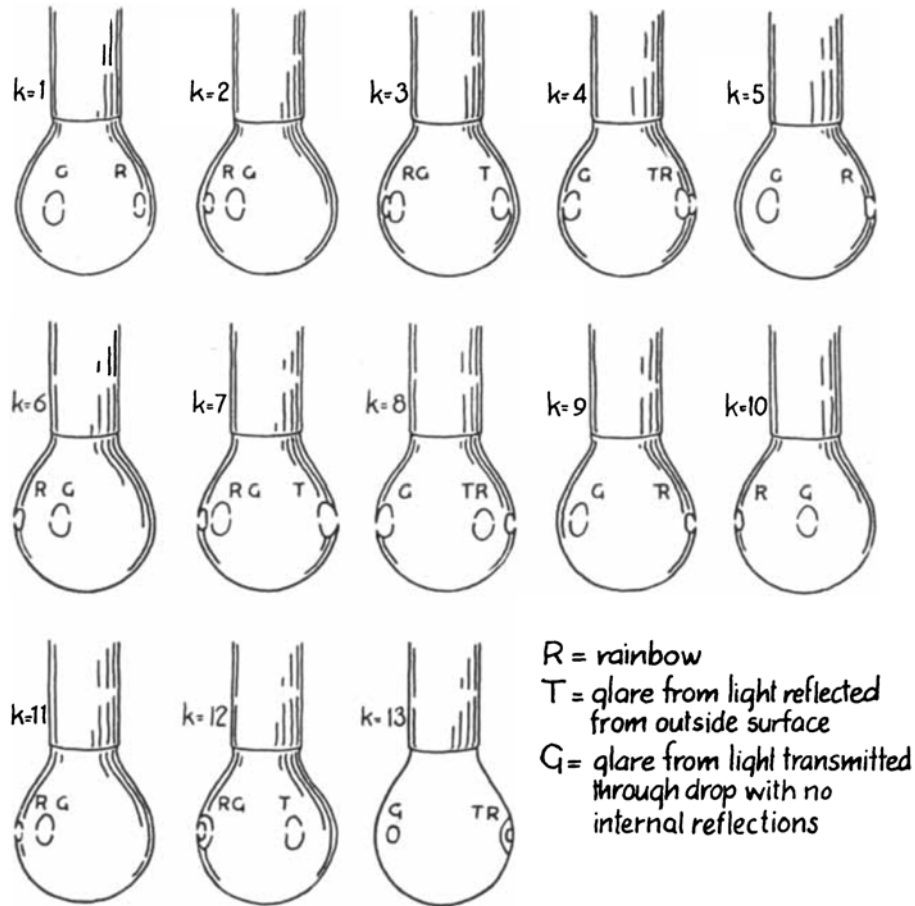
## A rainbow puzzle



Matthias Zscharnack



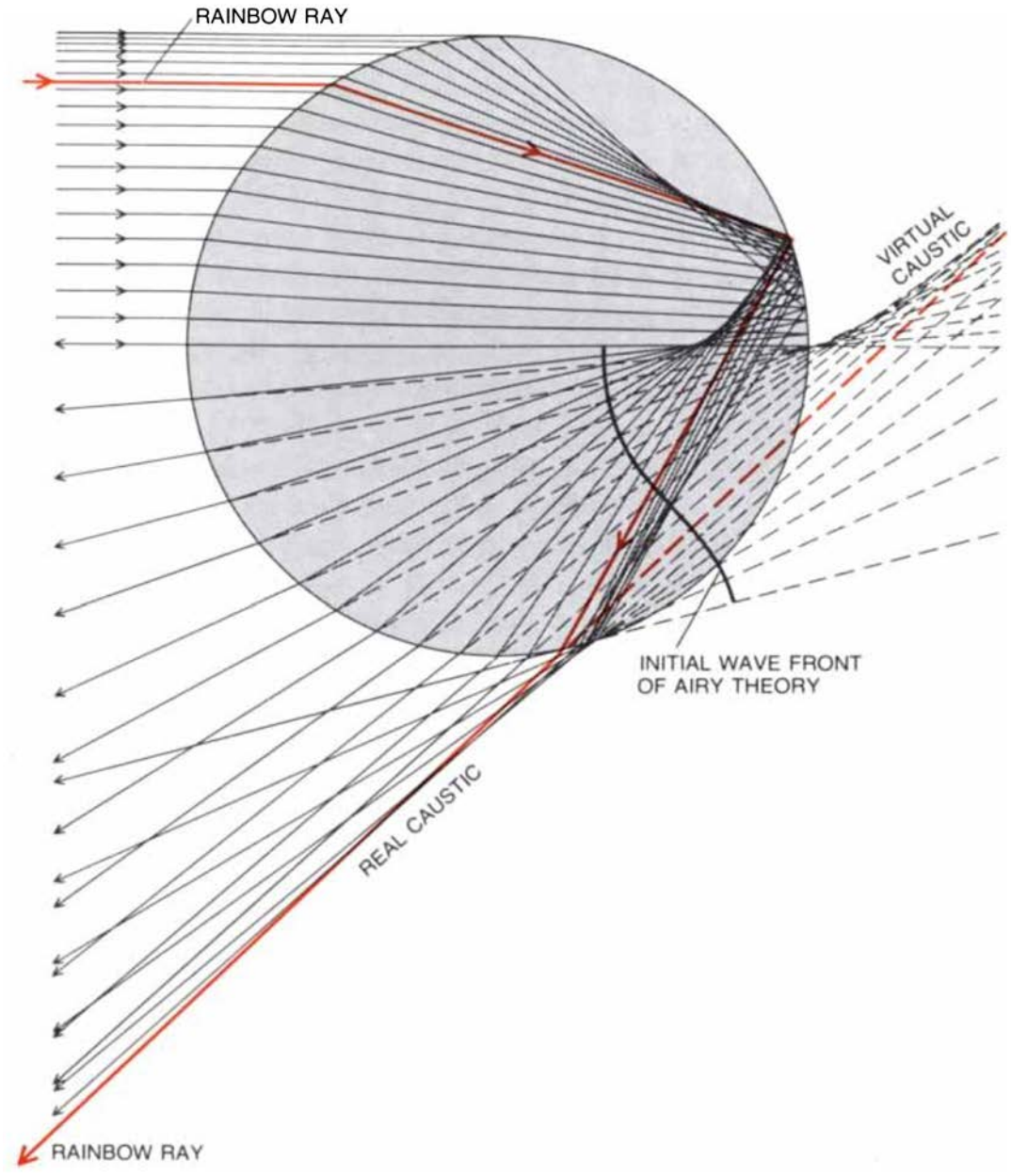
## Rainbow order



Appearance of the first 13 rainbows

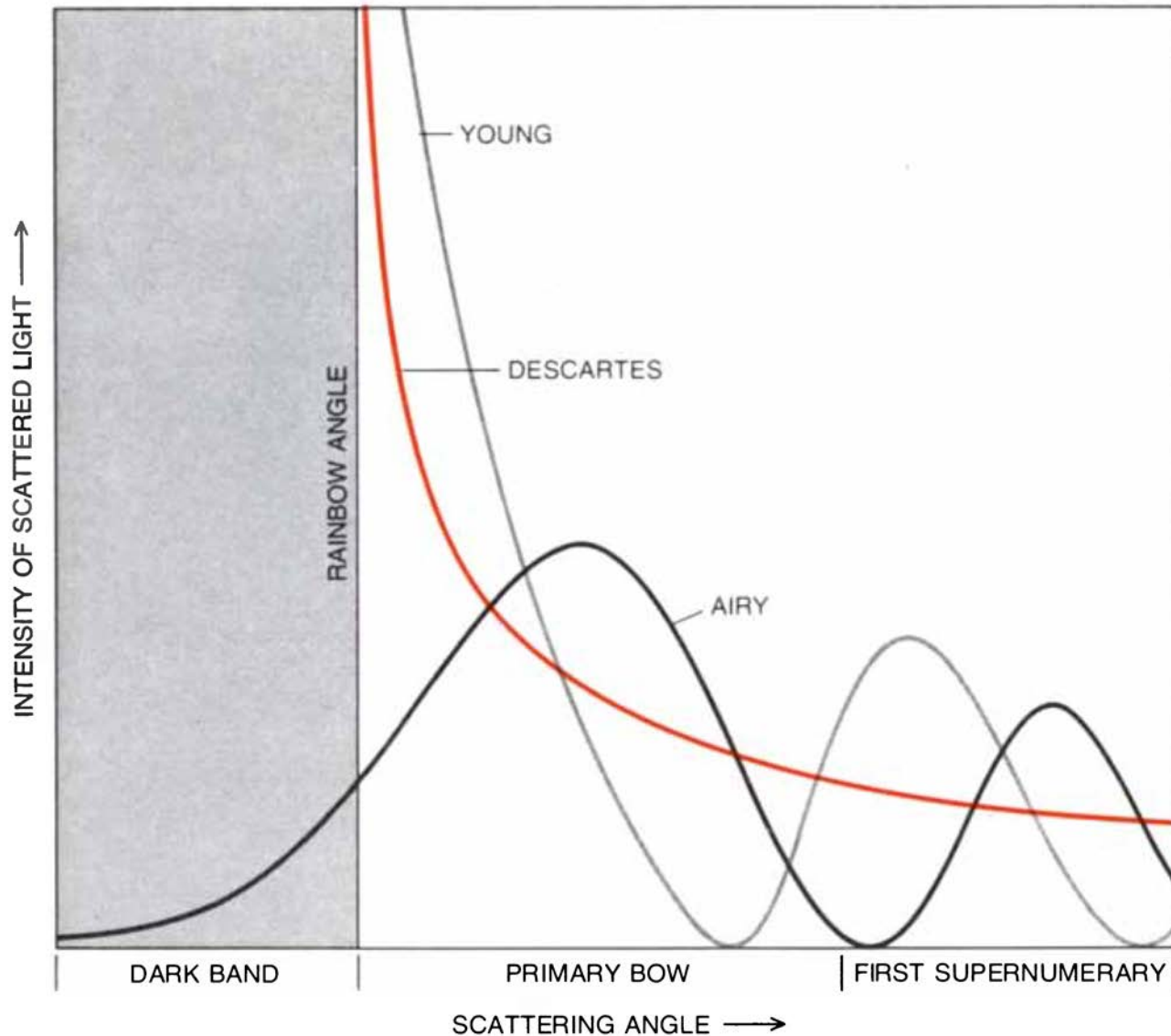
Rainbow order	Angular width	Red	Blue	Side of drop
1	1.72°	137.63°	139.35°	right
2	3.11	129.63	126.52	left
3	4.37	42.48	38.11	left
4	5.58	42.76	48.34	right
5	6.78	127.08	133.86	right
6	7.96	149.10	141.14	left
7	9.14	65.59	56.45	left
8	10.31	17.71	28.02	right
9	11.49	100.86	112.35	right
10	12.65	176.08	163.43	left
11	13.82	93.11	79.29	left
12	14.98	10.19	4.79	split
13	16.15	72.68	88.83	right
14	17.31	155.51	172.82	right
15	18.48	121.69	103.21	left
16	19.64	38.91	19.27	left
17	20.81	43.84	64.65	right
18	21.97	126.58	148.55	right
19	23.13	150.70	127.57	left
20	24.29	67.98	43.69	left

Calculated angles of the first 20 rainbows



"CONFLUENCE OF RAYS scattered by a droplet gives rise to caustics, or "burning curves." A caustic is the envelope of a ray system. Of special interest is the caustic of Class 3 rays, which has two branches, a real branch and a "virtual" one; the latter is formed when the rays are extended backward. When the rainbow ray is produced in both directions, it approaches the branches of this caustic. A theory of the rainbow based on the analysis of such a caustic was devised by George B. Airy. Having chosen an initial wave front – a surface perpendicular at all points to the rays of Class – Airy was able to determine the amplitude distribution in subsequent waves. A weakness of the theory is the need to guess the amplitudes of the initial waves."

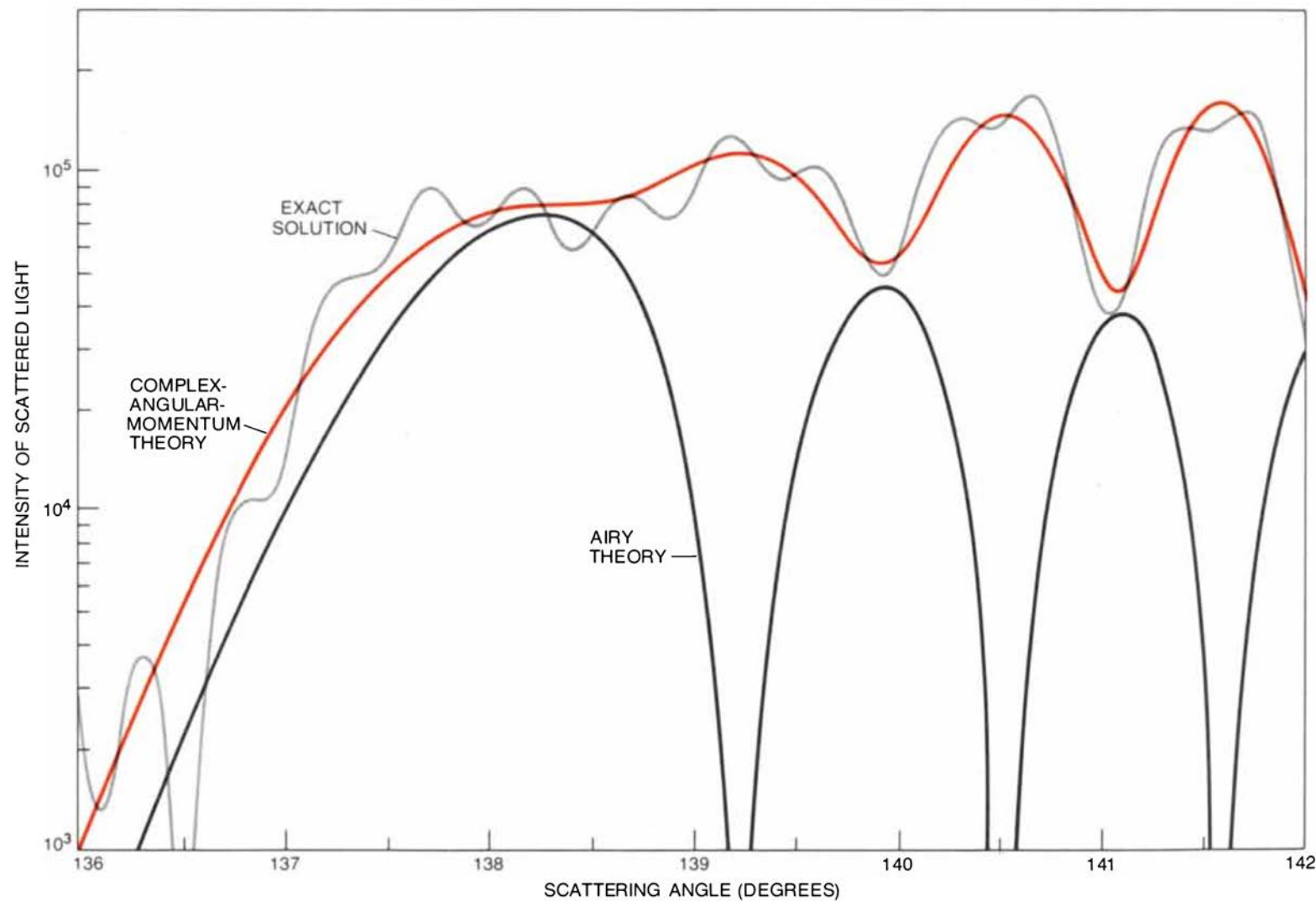
(from H. Moyses Nussenzveig: "Theory of the Rainbow", Sci. Am., April 1977)



PREDICTED INTENSITY as a function of scattering angle is compared for three early theories of the rainbow. In the geometric analysis of Descartes, intensity is infinite at the rainbow angle; it declines smoothly (without supernumerary arcs) on the lighted side and falls off abruptly to zero on the dark side. The theory of Thomas Young, which is based on the interference of light waves, predicts supernumerary arcs but retains the sharp transition from infinite to zero intensity. Airy's theory relocates the peaks in the intensity curve and for the first time provides (through diffraction) an explanation for gradual fading of the rainbow into shadow.

(from H. Moyses Nussenzveig: "Theory of the Rainbow", Sci. Am., April 1977)

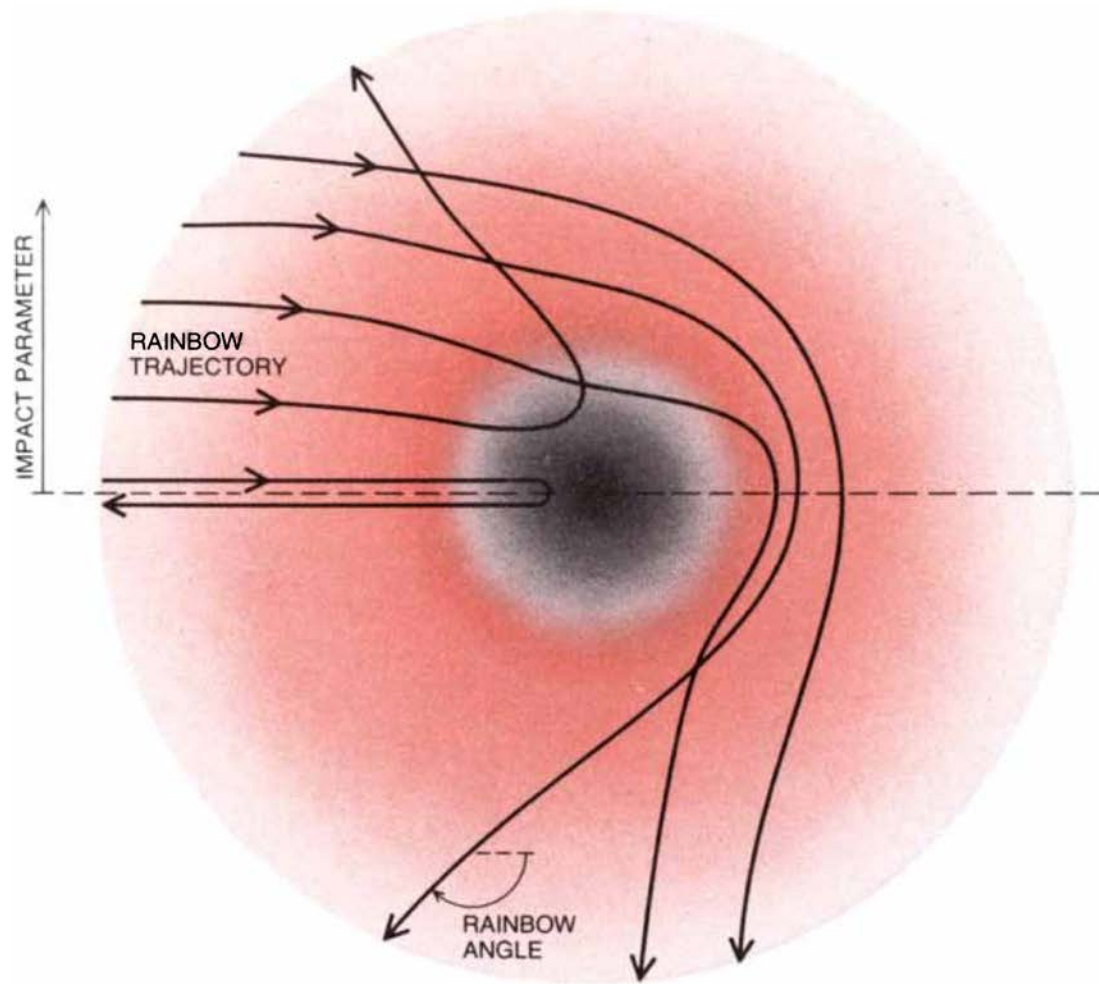




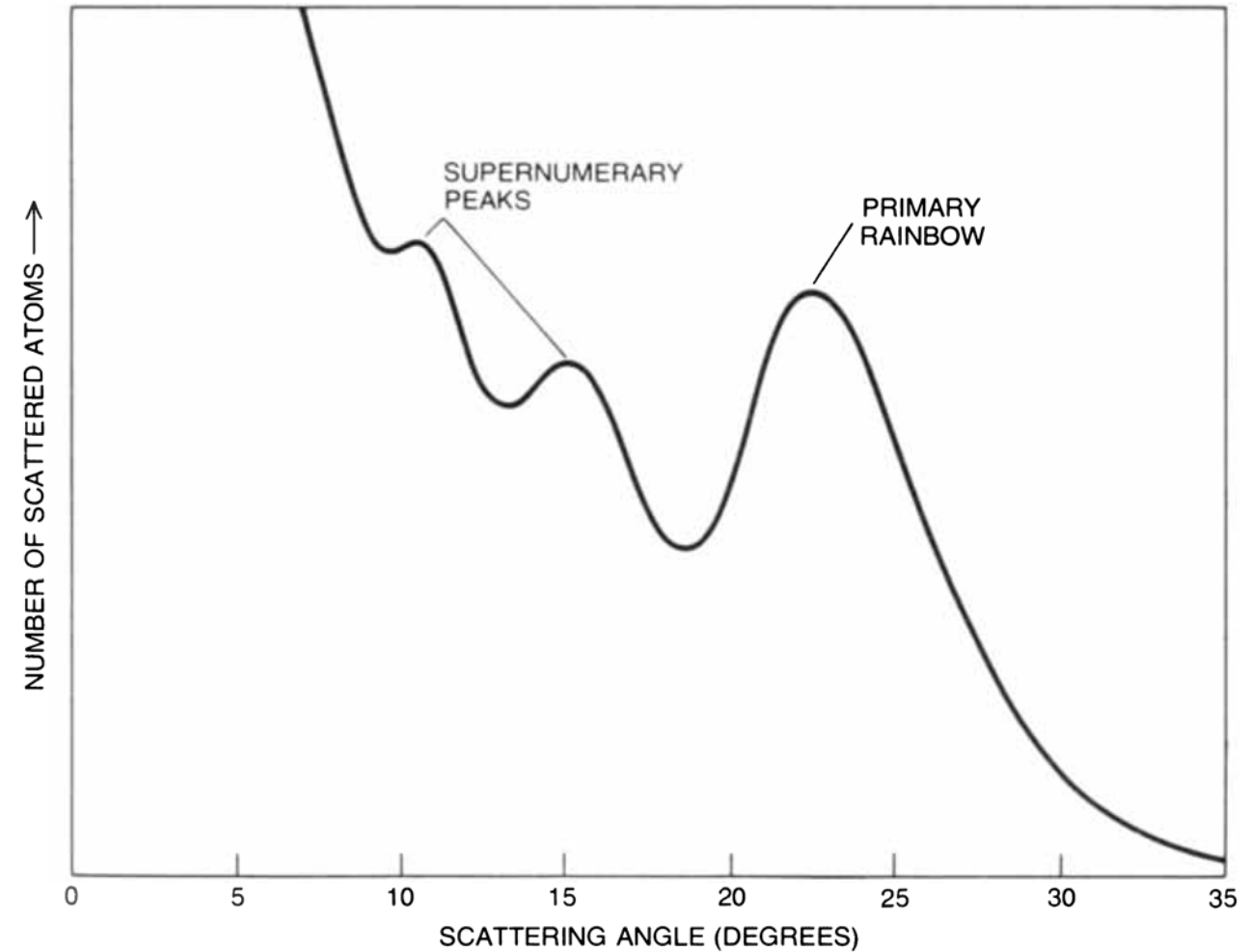
**QUANTITATIVE THEORIES** of the rainbow predict the intensity of the scattered light as a function of the scattering angle and also with respect to droplet size and polarization. Here the predictions of three theories are presented for parallel-polarized light scattered by droplets with a circumference equal to 1,500 wavelengths of the light. One curve represents the “exact” solution to the rainbow problem, derived from James Clerk Maxwell’s equations describing electromagnetic radiation. The exact solution is the sum of an infinite series of terms, approximated here by adding up more than 1,500 compli-

cated terms for each point employed in plotting the curve. The Airy theory is clearly in disagreement with the exact solution, particularly in the angular region of the supernumerary arcs. There the exact solution shows troughs at the positions of Airy’s peaks. The results obtained by the complex-angular-momentum method, on the other hand, correspond closely to the exact solution, failing only to reproduce small, high-frequency oscillations. These fluctuations are associated with another optical phenomenon in the atmosphere, the glory, which is also explained by the complex-angular-momentum theory.





**SCATTERING OF ATOMS BY ATOMS** creates a particulate rainbow. The role played in optical scattering by the refractive index is played here by interatomic forces. The principal difference is that the forces vary smoothly and continuously, so that the atoms follow curved trajectories. As one atom approaches another the force between them is initially a steadily growing attraction (*colored shading*), but at close range it becomes strongly repulsive (*gray shading*). A local maximum in the scattering angle corresponds to the optical rainbow angle. It is the angle made by the trajectory most effective in using the attractive part of the potential.



**ATOMIC RAINBOW** was detected by E. Hundhausen and H. Pauly of the University of Bonn in the scattering of sodium atoms by mercury atoms. The oscillations in the number of scattered atoms detected correspond to a primary rainbow and to two supernumerary peaks. A rainbow of this kind embodies information about the strength and range of the interatomic forces.

# Similarity between nuclear rainbow and meteorological rainbow: Evidence for nuclear ripples

S. Ohkubo<sup>1,\*</sup> and Y. Hirabayashi<sup>2</sup>

<sup>1</sup>*Research Center for Nuclear Physics, Osaka University, Ibaraki, Osaka 567-0047, Japan*

<sup>2</sup>*Information Initiative Center, Hokkaido University, Sapporo 060-0811, Japan*

(Received 14 May 2014; revised manuscript received 10 June 2014; published 27 June 2014)

We present evidence for the nuclear ripples superimposed on the Airy structure of the nuclear rainbow, which is similar to the meteorological rainbow. The mechanism of the nuclear ripples is also similar to that of the meteorological rainbow, which is caused by the interference between the externally reflective waves and refractive waves. The nuclear ripple structure was confirmed by analyzing the elastic angular distribution in  $^{16}\text{O} + ^{12}\text{C}$  rainbow scattering at  $E_L = 115.9$  MeV using the coupled channels method by taking account of coupling to the excited states of  $^{12}\text{C}$  and  $^{16}\text{O}$  with a double folding model derived from a density-dependent effective nucleon-nucleon force with realistic wave functions for  $^{12}\text{C}$  and  $^{16}\text{O}$ . The coupling to the excited states plays the role of creating the external reflection.

DOI: [10.1103/PhysRevC.89.061601](https://doi.org/10.1103/PhysRevC.89.061601)

PACS number(s): 25.70.Bc, 24.10.Eq, 42.25.Gy

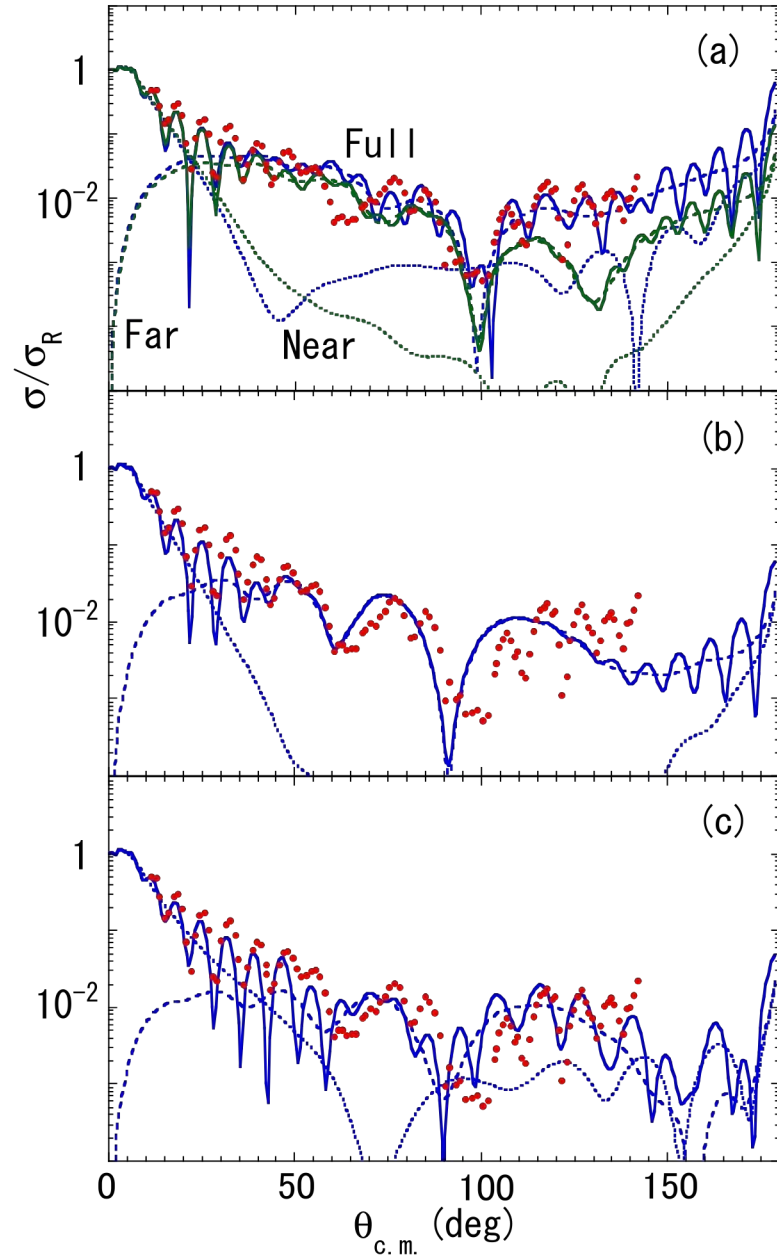
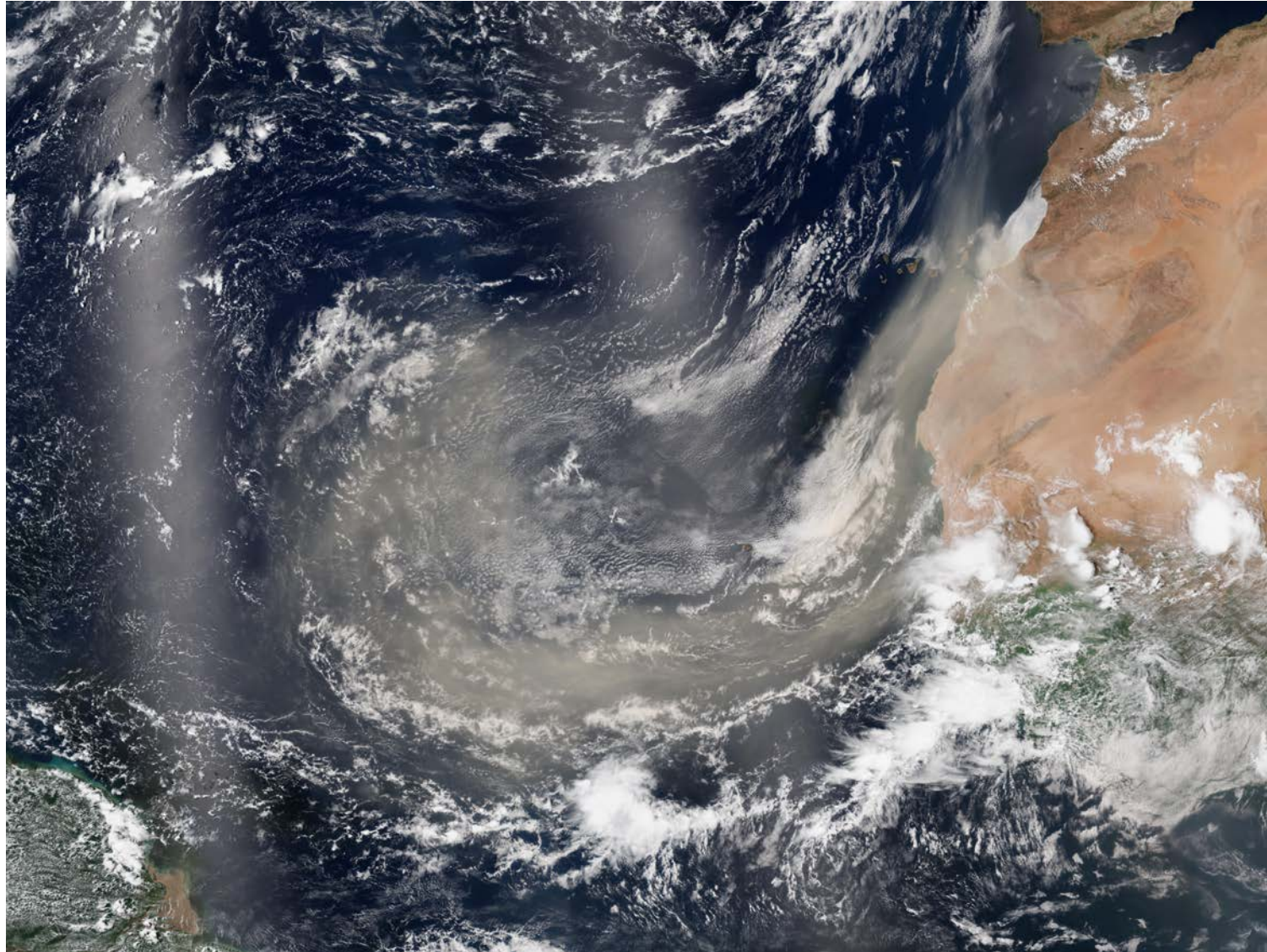


FIG. 3. (Color online) The experimental cross sections (points) in  $^{16}\text{O} + ^{12}\text{C}$  scattering at  $E_L = 115.9$  MeV [23] are compared with the calculations (solid line) using the EDF potential: (a) the coupled channels calculations with  $a_W = 0.2$  (blue line), (b) the single channel calculations with  $a_W = 0.6$ , and (c) the single channel calculations using the extremely thin-skinned volume-type imaginary potential with  $a_W = 0.1$ . For comparison, in (a) the coupled channels calculations with  $a_W = 0.4$  are displayed by the green line. The calculated cross sections (solid line) are decomposed into the farside (dashed line) and nearside (dotted line) components.

from S. Ohkubo and Y. Hirabayashi, PRC **89**, 061601(R) (2014)

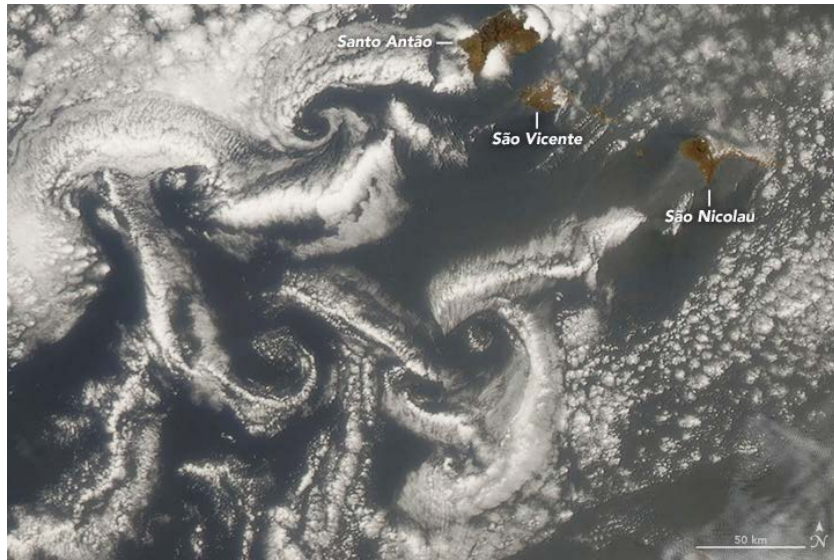


# The global transport of dust



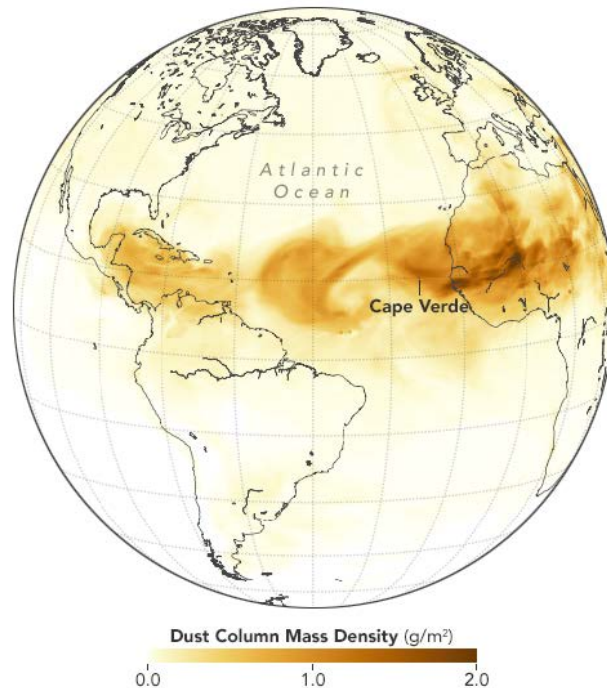
End of July 2013 Saharan sand outbreak  
from <https://visibleearth.nasa.gov/view.php?id=81864>





The Sahara Desert, the Caribbean, and Texas may be several thousand miles apart, but a massive cloud of dust connected these places in late June 2018.

On June 18, satellites began to detect thick plumes of Saharan dust passing over Mauritania, Senegal, Gambia, and Guinea-Bissau before moving out over the Atlantic Ocean. For the next ten days, the skies over West Africa and across the tropical Atlantic were stained a distinctive shade of yellow as winds pushed pulse after pulse of Saharan dust to the west. According to one preliminary analysis, this brought the tropical Atlantic one of its dustiest weeks in 15 years.



The map shows dust crossing the Atlantic on June 28, 2018, as represented by the Goddard Earth Observing System Model, Version 5 (GEOS-5). A simulation from GEOS-5 shows plumes of dust from as far away as Iraq and Saudi Arabia blowing across North Africa in mid-June. However, much of the dust that crossed the Atlantic Ocean appeared to be coming from the Bodele depression, a dried lake bed in northeastern Chad.

From <https://visibleearth.nasa.gov/view.php?id=92358>

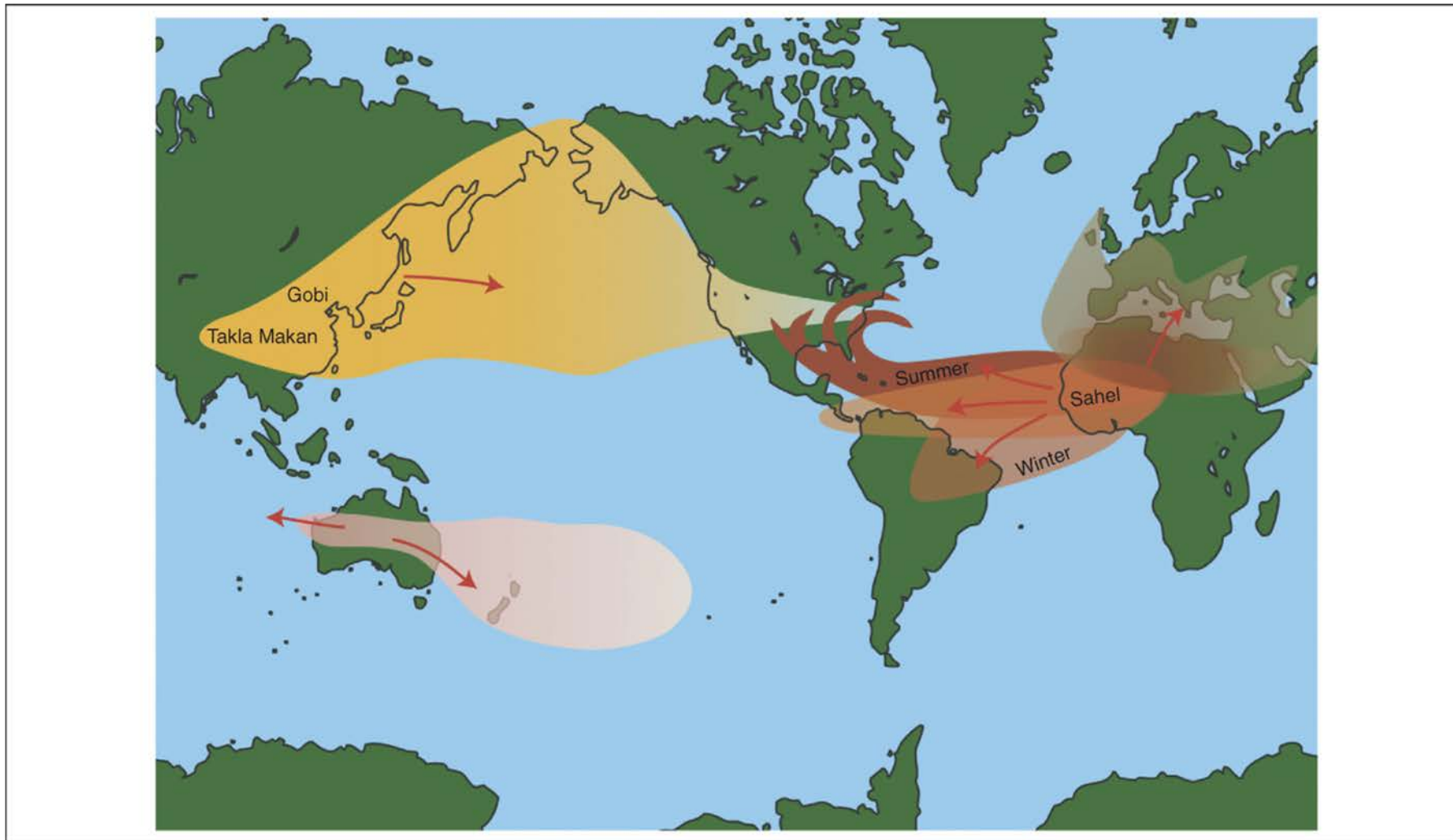
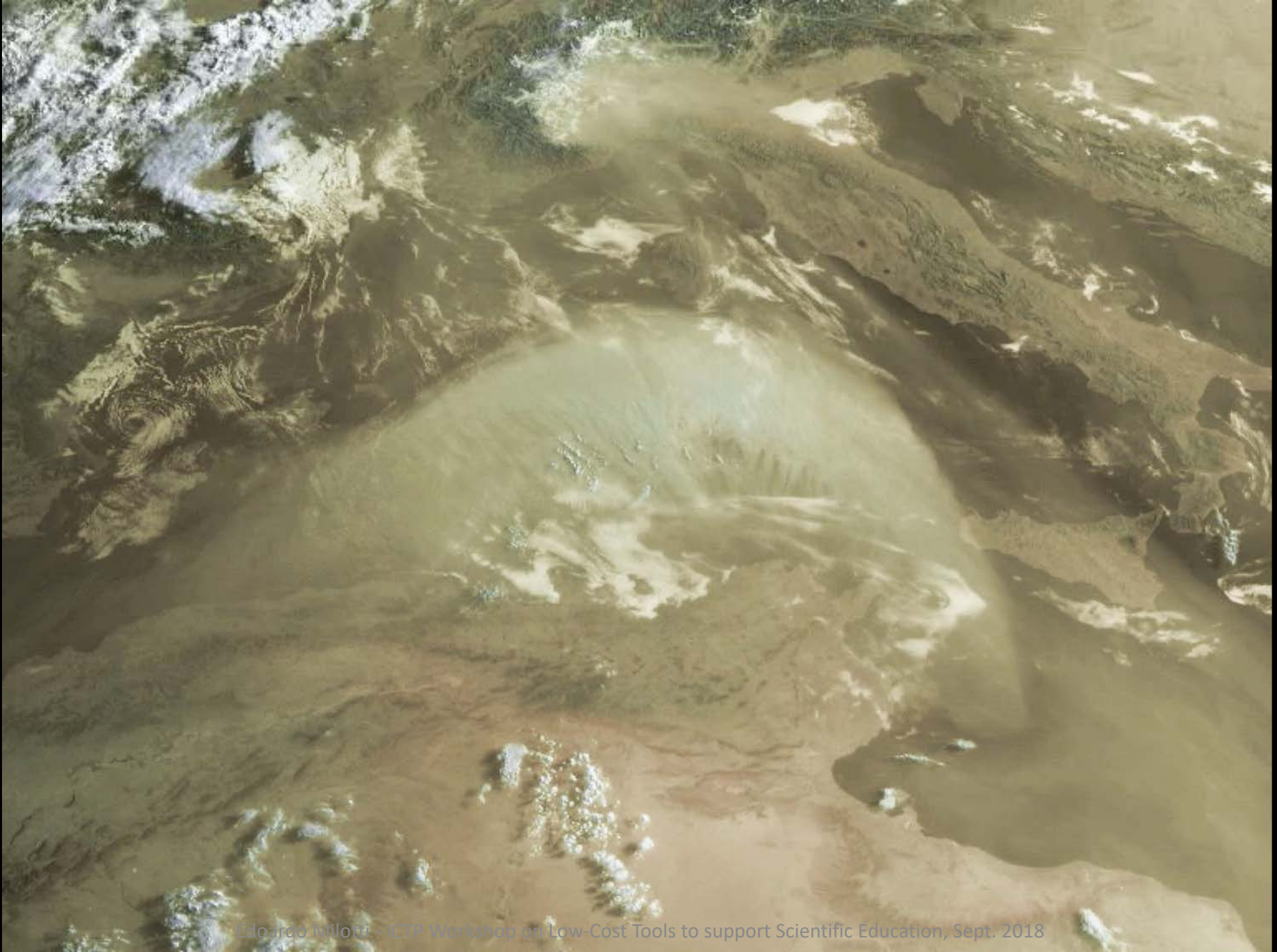


**Figure 2.** Principal ranges of the two major global dust transport systems. The African dust system (red-orange) has a strong seasonal component; in the summer (c. May–November) trade winds carry Saharan dust to the Caribbean and USA. In the winter (c. December–April) the African dust-flow is shifted to South America, where air-plants in the Amazon rainforest derive nutrients from the dust. Throughout the year, pulses of dust from northern Africa cross into the Mediterranean and Europe, impacting air quality. The Asian dust system (yellow) exports dust primarily during the spring (March–May). These dust events can incorporate emissions from factories in China, Korea and Japan, carrying a ‘brown smog’ across the Pacific to the west coast of North America. Occasionally, extremely large Asian dust events can travel across the entire USA and then impact Europe, making an almost complete circuit of the globe. Although not an intercontinental dust source, Australian deserts (pink) produce large dust storms that can reach New Zealand and halfway to South America. This updated version of a figure from [9] is reproduced with permission.



Meteosat-8 video, July 28 2005

[http://oiswww.eumetsat.org/WEBOPS/iotm/iotm/20050728\\_dust/20050728\\_dust.html](http://oiswww.eumetsat.org/WEBOPS/iotm/iotm/20050728_dust/20050728_dust.html)



*" ... When it comes to Saharan dust outbreaks, the photovoltaic output is reduced not only through a significant increase in atmospheric aerosol content by 10 to 20 percent, but also through dust deposition on the photovoltaic modules on subsequent days. ..."*

from the Karlsruhe Institute of Technology press release 103, July 2016



*Measurements carried out at KIT will determine the effect of soiled solar panels on the output of photovoltaic systems caused by deposited mineral dust. (Photo: Sandra Göttisheim)*



## Bacterial diversity and composition during rain events with and without Saharan dust influence reaching a high mountain lake in the Alps

Hannes Peter,<sup>1</sup> Paul Hörtnagl,<sup>1</sup> Isabel Reche<sup>2</sup> and Ruben Sommaruga<sup>1\*</sup>

<sup>1</sup>*Institute of Ecology, Alpine Freshwater Ecology Division, Lake and Glacier Research Group, University of Innsbruck, Technikerstr. 25, Innsbruck 6020, Austria.*

<sup>2</sup>*Department of Ecology, University of Granada, Granada 18071, Spain.*

### Summary

The diversity of airborne microorganisms that potentially reach aquatic ecosystems during rain events is poorly explored. Here, we used a culture-independent approach to characterize bacterial assemblages during rain events with and without Saharan dust influence arriving to a high mountain lake in the Austrian Alps. Bacterial assemblage composition differed significantly between samples with and without Saharan dust influence. Although alpha diversity indices were within the same range in both sample categories, rain events with Atlantic or continental origins were dominated by Betaproteobacteria, whereas those with Saharan dust intrusions were dominated by Gammaproteobacteria. The high diversity and evenness observed in all samples suggests that different sources of bacteria contributed to the airborne assemblage collected at the lake shore. During experiments with bacterial assemblages collected during rain events with Saharan dust influence, cell numbers rapidly increased in sterile lake water from initially  $\sim 3 \times 10^3$  cell ml<sup>-1</sup> to  $3.6\text{--}11.1 \times 10^5$  cells ml<sup>-1</sup> within 4–5 days, and initially, rare taxa dominated at the end of the experiment. Our study documents the dispersal of viable bacteria associated to Saharan dust intrusions travelling northwards as far as 47° latitude.



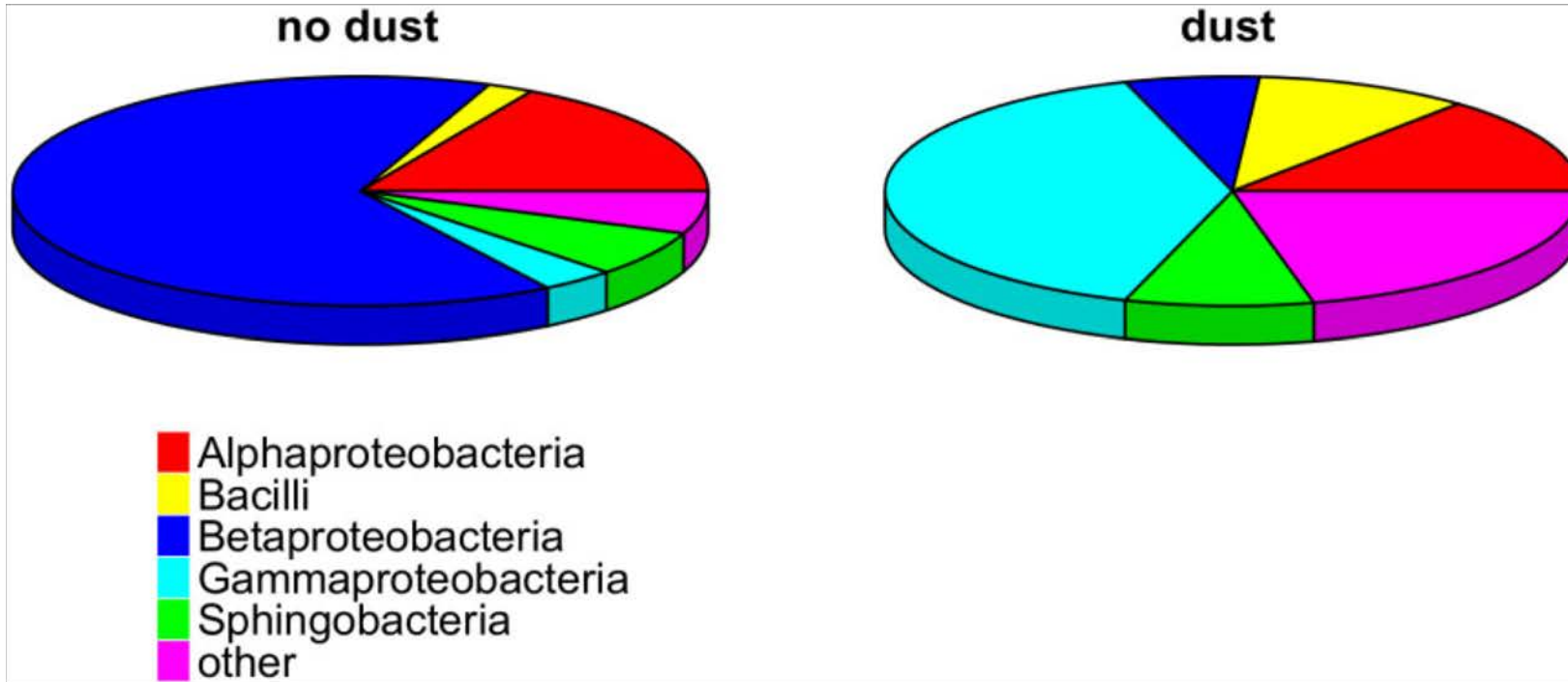


**Fig. 2.** Pie charts showing the relative contribution of common bacterial classes to overall diversity in rain samples with and without Sahara dust influence. Colours indicate operational taxonomic unit class affiliation.

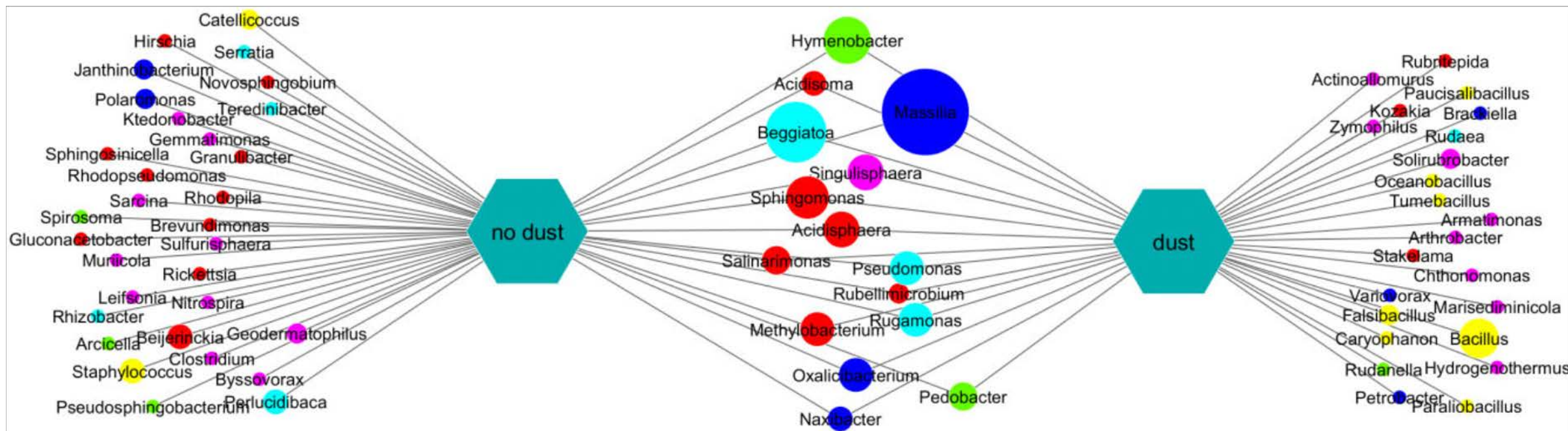


**Fig. 3.** Operational taxonomic unit (OTU) level representation of bacterial sequences retrieved from samples collected during rain events with and without Saharan dust intrusions. Circles represent OTUs, and lines indicate the occurrence of an OTU in the respective samples. Circle size reflects log-transformed sequence abundance, while colour indicates taxonomic affiliation (see Fig. 2 for key). While several abundant sequences were found in samples with and without Saharan dust influence, *Bacillus*, *Falsibacillus* and *Solorubrobacter* were exclusively found during Saharan dust intrusions and dominated these samples. The diversity of OTUs retrieved exclusively during rain events without dust appears larger, and no taxon was distinctively dominant in those samples.

# More measurements ...

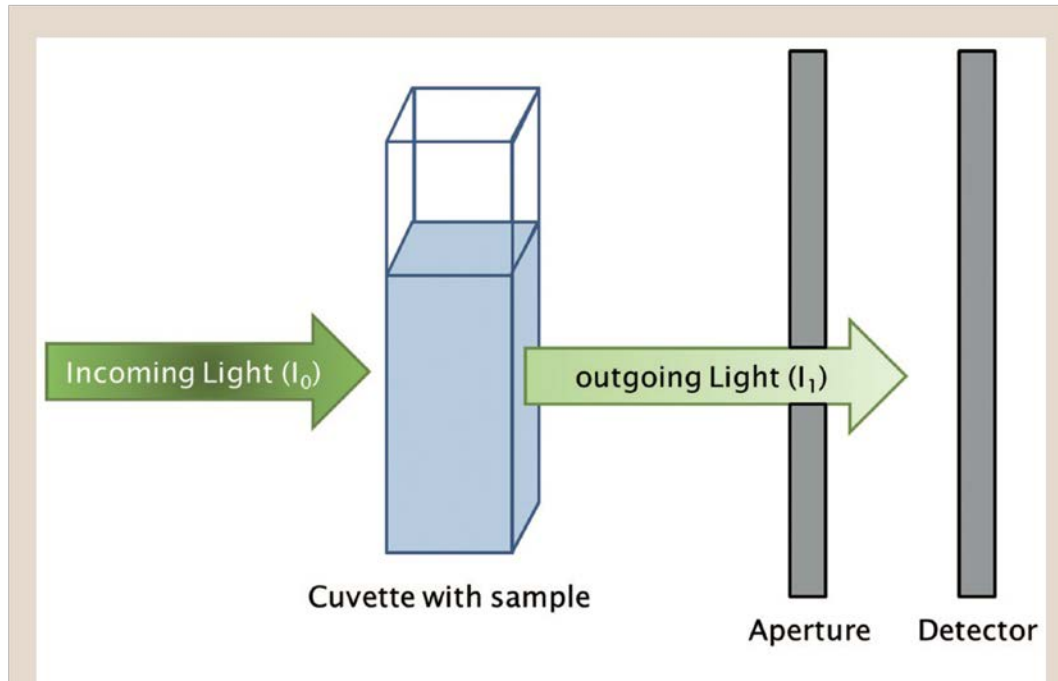


**Figure 1:** Typical set up of an absorbance measurement in a photometer. The incoming light intensity is reduced by absorption of sample molecules and this reduced light intensity is measured at the detector. By comparing the incoming and outgoing amount of light the concentration of a sample is calculated.

from Eppendorf White Paper No. 28, Sept. 2015

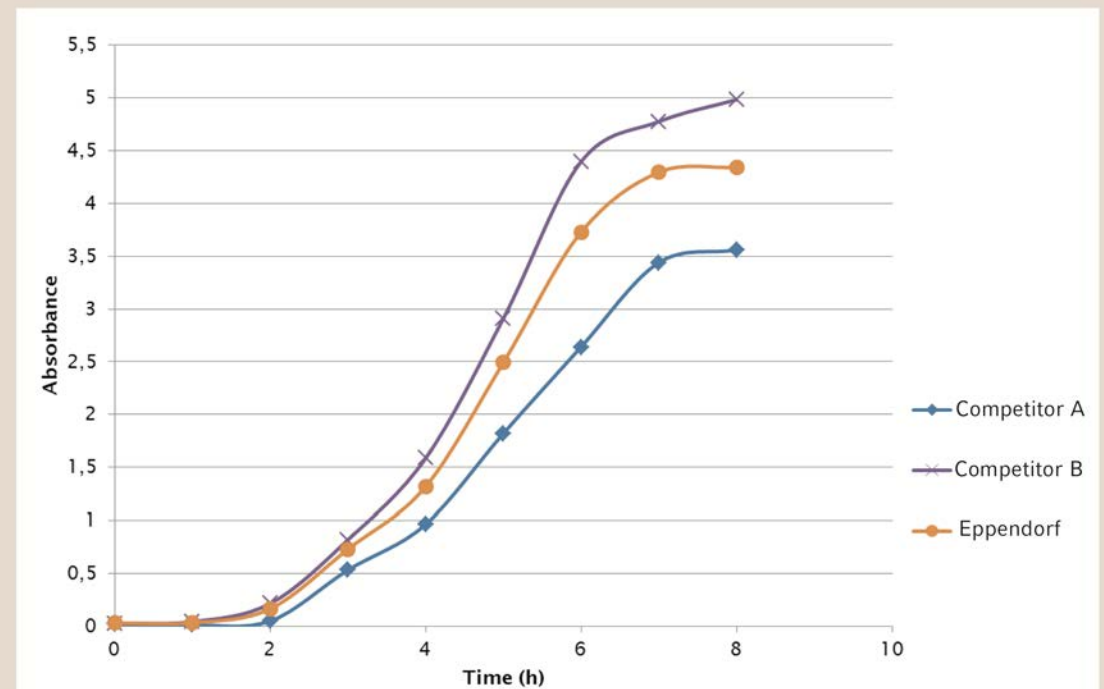


**Figure 2:** Growth curves of *E. coli* DH5α grown in LB medium for 8 h shaking at 180 rpm at 37 °C. Every 60 min the OD600 of the same sample was measured in three different photometers showing that the results differ when comparing different instruments. The samples were diluted using LB medium when an absorbance value of 0.8 was reached to guarantee accurate measuring at 600 nm. The dilution factor was used to multiply with the measured result for absorbance value determination.

# Photometer project

- Start from simple electronics to build an instrument that allows simple quantitative optical measurements
- Many applications
- Use the sun photometer to find local/global atmospheric absorption